Alan L. Deino
Berkeley Geochronology Center, 2455 Ridge Road, Berkeley, CA 94709, U.S.A.
E-mail: al@bgc.org

Sally McBrearty
Department of Anthropology, University of Connecticut, Storrs, CT 06269, U.S.A.
E-mail: mcbrearty@uconn.edu

Received 1 March 2001
Revision received
18 July 2001 and
accepted 5 September 2001

Keywords: geochronology, radioisotopic dating, Middle Pleistocene, East Africa, Acheulian, Middle Stone Age.

$^{40}Ar/^{39}Ar$ dating of the Kapthurin Formation, Baringo, Kenya

The $^{40}Ar/^{39}Ar$ radiometric dating technique has been applied to tuffs and lavas of the Kapthurin Formation in the Tugen Hills, Kenya Rift Valley. Two variants of the $^{40}Ar/^{39}Ar$ technique, single-crystal total fusion (SCTF) and laser incremental heating (LIH) have been employed to date five marker horizons within the formation: near the base, the Kasurein Basalt at $0{\cdot}61 \pm 0{\cdot}04$ Ma; the Pumice Tuff at $0{\cdot}543 \pm 0{\cdot}004$ Ma; the Upper Kasurein Basalt at $0{\cdot}552 \pm 0{\cdot}015$ Ma; the Grey Tuff at $0{\cdot}509 \pm 0{\cdot}009$ Ma; and within the upper part of the formation, the Bedded Tuff at $0{\cdot}284 \pm 0{\cdot}012$ Ma. The new, precise radiometric age determination for the Pumice Tuff also provides an age for the widespread Lake Baringo Trachyte, since the Pumice Tuff is the early pyroclastic phase of this voluminous trachyte eruption.

These results establish the age of fossil hominids KNM-BK 63-67 and KNM-BK 8518 at approximately 0·510–0·512 Ma, a significant finding given that few Middle Pleistocene hominids are radiometrically dated. The Kapthurin hominids are thus the near contemporaries of those from Bodo, Ethiopia and Tanzania. A flake and core industry from lacustrine sediments in the lower part of the formation is constrained by new dates of 0·55–0·52 Ma, a period during which the Acheulian industry, characterized by handaxes, is known throughout East Africa. Points, typical of the Middle Stone Age (MSA), are found in Kapthurin Formation sediments now shown to date to between $0{\cdot}509 \pm 0{\cdot}009$ Ma and $0{\cdot}284 \pm 0{\cdot}012$ Ma. This date exceeds previous estimates for the age of the MSA elsewhere in East Africa by 49 ka, and establishes the age of Acheulian to MSA transition for the region. Evidence of the use of the Levallois technique for the manufacture of both small flakes and biface preforms, the systematic production of blades, and the use and processing of red ochre also occurs in this interval. The presence of blades and red ochre at this depth is important as blades signify a high degree of technical competence and red ochre suggests symbolic behavior.

Journal of Human Evolution (2002) **42,** 185–210
doi:10.1006/jhev.2001.0517
Available online at http://www.idealibrary.com on IDEAL®

Introduction

The African Middle Pleistocene fossil record preserves the earliest traces of *Homo sapiens*. Profound changes in hominid behavior during this time interval are implied by the disappearance of Acheulian technology and its replacement by diverse Middle Stone Age (MSA) traditions. Few Middle Pleistocene sites in Africa are well dated, and as a result the timing of events is not well known. The Kapthurin Formation spans a significant portion of the Middle Pleistocene, contains many artifacts and fossils, including hominids, and is punctuated by volcanic units that can be accurately dated by the $^{40}Ar/^{39}Ar$ technique. The new age calibration of the Kapthurin Formation reported in this study establishes a precise age for Kapthurin hominids, for the Acheulian–MSA transition, and for the first appearance of several key behavioral

0047–2484/02/010185+26$35.00/0

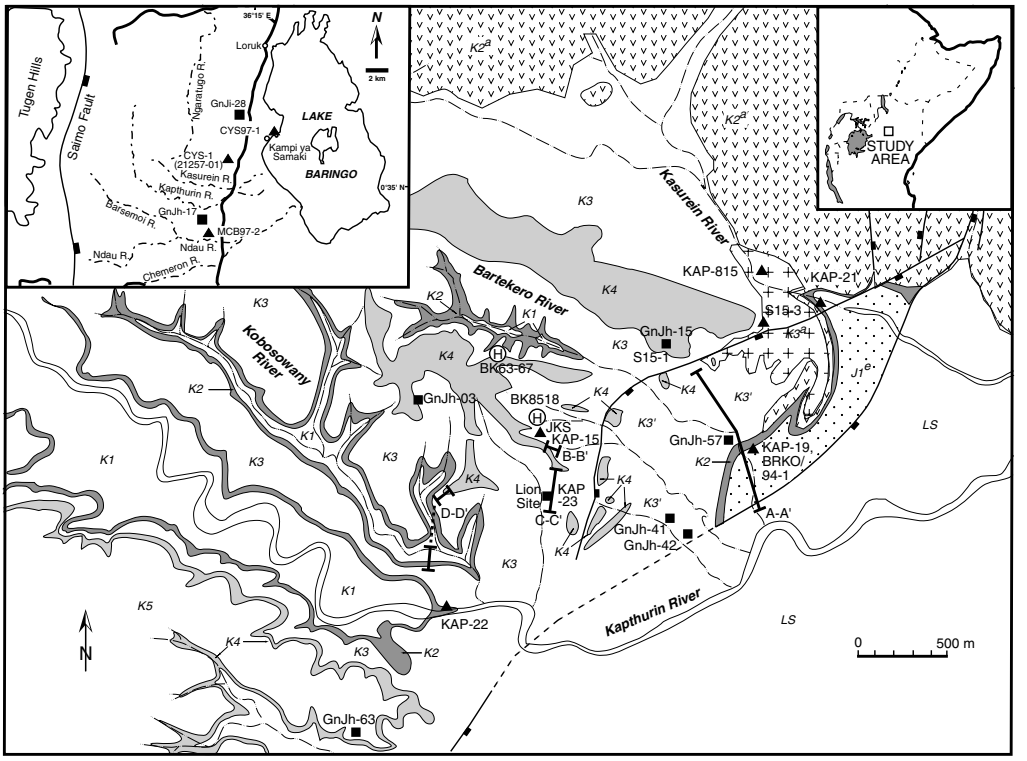

Figure 1. Geologic map of the study area, indicating extent of outcrop of sampled volcanic units, locations of measured sections (A-A′, B-B′, etc.), archaeological sites (GnJh and GnJi numbers), hominid fossils (BK numbers), and $^{40}Ar/^{39}Ar$ sampling localities (all other numbers). Refer to Figure 2 for key to geologic units (K1, K2, etc.).

markers, most notably the development of the Levallois technique of flake production, the manufacture of blades, and the apparent use and processing of red ochre.

The Kapthurin Formation

The Kapthurin Formation forms part of the Tugen Hills sedimentary sequence, exposed in a 75 km long, north–south oriented complex tilted fault block jutting from the floor of the Kenya rift. The 125–150 m-thick formation is exposed over an area of about 150 km^2, lying between the crest of the Tugen Hills to the west, and modern Lake Baringo to the east (Figure 1). The region has been studied by geologists for over a hundred years (Thomson, 1884; Gregory, 1896), and has been recognized as fossiliferous since the 1940s (Fuchs, 1950). The area was mapped by the Geological Survey of Kenya (Walsh, 1969) and the East African Geological Research Unit (EAGRU) (e.g., Martyn, 1969; Bishop *et al.*, 1971; Chapman *et al.*, 1978), and since about 1980 more detailed local sequences have been documented by the Baringo Paleontological Research Project (BPRP) (e.g., Hill *et al.*, 1985, 1986). The intercalated volcanics have permitted construction of a chronostratigraphy based on conventional K/Ar dating, $^{40}Ar/^{39}Ar$ dating, and paleomagnetism for the Tugen Hills volcanosedimentary sequence spanning the period ca. 14–1·6 Ma (Tauxe *et al.*, 1985; Hill *et al.*, 1986; Deino *et al.*, 1990; Deino & Hill, 2002).

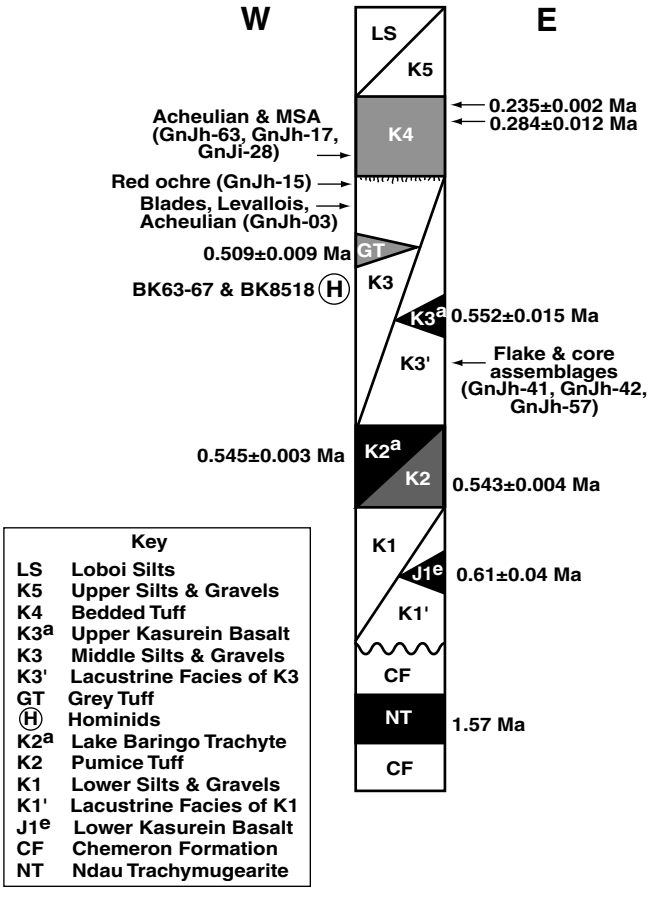

Figure 2. Generalized stratigraphic section for the Kapthurin Formation, modified after Tallon (1976). All dates result from ^{40}Ar/^{39}Ar analysis reported here, with the exception of the Ndau trachymugearite (NT), dated by Hill *et al.* (1986).

Sedimentary rocks now referred to the Kapthurin Formation were part of the type section for the "Kamasian pluvial" of Leakey (1955). The "Kamasian" beds were divided into the early Pliocene Chemeron Formation and Middle Pleistocene Kapthurin Formation by McCall *et al.* (1967). Martyn (1969) subdivided the Kapthurin Formation into five major units (K1 through K5; Figure 2), with refinements by Tallon (1976, 1978). Members K1, K3, and K5, termed the Lower, Middle, and Upper Silts and Gravels by Martyn, are primarily of fluviolacustrine sedimentary origin. The sedimentary rocks of members K1, K3, and K5 are derived primarily from the Miocene and Pliocene rocks of the Tugen Hills to the west, and the rate of accumulation has been controlled in part by activity along the north-south trending Saimo fault (see Figure 1). The Kapthurin Formation is well exposed in the valleys of streams that drain the Tugen Hills and debouch into the main axis of the rift (Figure 1).

Volcaniclastic tuffs and lava flows intercalated within the Kapthurin Formation at several levels provide potential resources for radioisotopic dating, and volcanic units underlying the formation also offer valuable age constraints.

Previous attempts to constrain the maximum age of the Kapthurin Formation have relied on K–Ar ages for the Lower Kasurein Basalt, intercalated within K1 close to the base of the formation, and on lavas which underlie the Kapthurin Formation with angular discordance. Cornelissen *et al.* (1990) reports ages ranging from 1·5–1·1 Ma on the Lower Kasurein Basalt, concluding that an age of 1·2 Ma is probably closest to reality. The stratigraphically older, structurally disconformable lavas (Ndau trachy-mugearite, Songoiwa trachy-mugearite) are apparently 1·6 Ma or older (Hill *et al.*, 1986; Cornelissen *et al.*, 1990; Deino & Hill, 2002). However, the entire Kapthurin Formation appears to be normally magnetized (Dagley *et al.*, 1978; Cornelissen *et al.*, 1990), indicating that it is probably younger than 791 ka, the radioisotopic age of the Brunhes/Matuyama boundary (Yamei *et al.*, 2000; Singer & Pringle, 1996, adjusted for Renne *et al.*, 1998).

The pyroclastic air-fall "Pumice Tuff" (K2) and its overlying lava flow, the Lake Baringo Trachyte, have been long recognized as being emplaced during the same eruptive sequence based on field evidence (Martyn, 1969; Tallon, 1976). This evidence includes direct contact of the Lake Baringo Trachyte on top of Pumice Tuff without evidence of weathering; large Lake Baringo Trachyte-like lava blocks enclosed completely within Pumice Tuff, and coarsening of trachyte bombs and lava fragments in the Pumice Tuff northward toward the inferred source of the Lake Baringo Trachyte, a few kilometers north of the flow's southern edge (Martyn, 1969; Tallon, 1976). Previously reported K–Ar ages on the Pumice Tuff (K2) are between $0{\cdot}62 \pm 0{\cdot}06$ and $0{\cdot}867 \pm 0{\cdot}259$ Ma (J. A. Miller cited in Tallon, 1976, see note in Table 1 concerning use of old and new isotopic constants; Cornelissen *et al.*, 1990). Cornelissen *et al.* (1990, Table 1) report 11 K–Ar ages on seven samples of the Lake Baringo Trachyte, ranging from $0{\cdot}40 \pm 0{\cdot}06$ to $0{\cdot}84 \pm 0{\cdot}03$ Ma. They select one of these samples, dated to $0{\cdot}58 \pm 0{\cdot}04$ Ma, to represent the age of the flow (Cornelissen *et al.*, 1990). This result is in disagreement with earlier K–Ar determinations for the Lake Baringo Trachyte of 0·230 Ma (Tallon, 1976) and 0·26 Ma (Chapman & Brook, 1978), reported merely as citations from J. Miller without analytical data or uncertainty.

Near the Kasurein River (Figure 1), the Lake Baringo Trachyte is overlain by sediments ~0·5 m thick, which in turn are overlain by the Upper Kasurein Basalt (Figure 3). Eight attempts to date the Upper Kasurein Basalt by whole-rock K/Ar reported by Cornelissen *et al.* (1990) resulted in a range of apparent ages from $0{\cdot}69 \pm 0{\cdot}09$ to $1{\cdot}16 \pm 0{\cdot}21$ Ma. Their best estimate for the age of this unit is 0·8 Ma.

The Grey Tuff occurs within the Middle Silts and Gravels (K3). It is discontinuously exposed in the study area over an area of only ~6 ha in several small drainages between the Bartekero and Kobosowany Rivers, and can be observed in section at the "JKS" site in the Bartekero River drainage (GnJh-20) and at the "Lion Site" (GnJh-23). The tuff crops out southwest of exposures of the Upper Kasurein Basalt, and the relative stratigraphic relationship of these two units is unknown.

Throughout the study area, the Middle Silts and Gravels (K3) are overlain by a succession of mafic volcaniclastic tuffs, in places intercalated with sediments, referred to as the Bedded Tuff (K4) (Tallon, 1976). No previous radioisotopic dates on the Bedded Tuff are available. However, our recent field investigations and chemical characterizations of the Bedded Tuff (Tryon & McBrearty, 2002) have identified a siliceous, anorthoclase-bearing tuff in the upper part of the unit in the southern part of the study area that provides a new, precise minimum age constraint for the Formation.

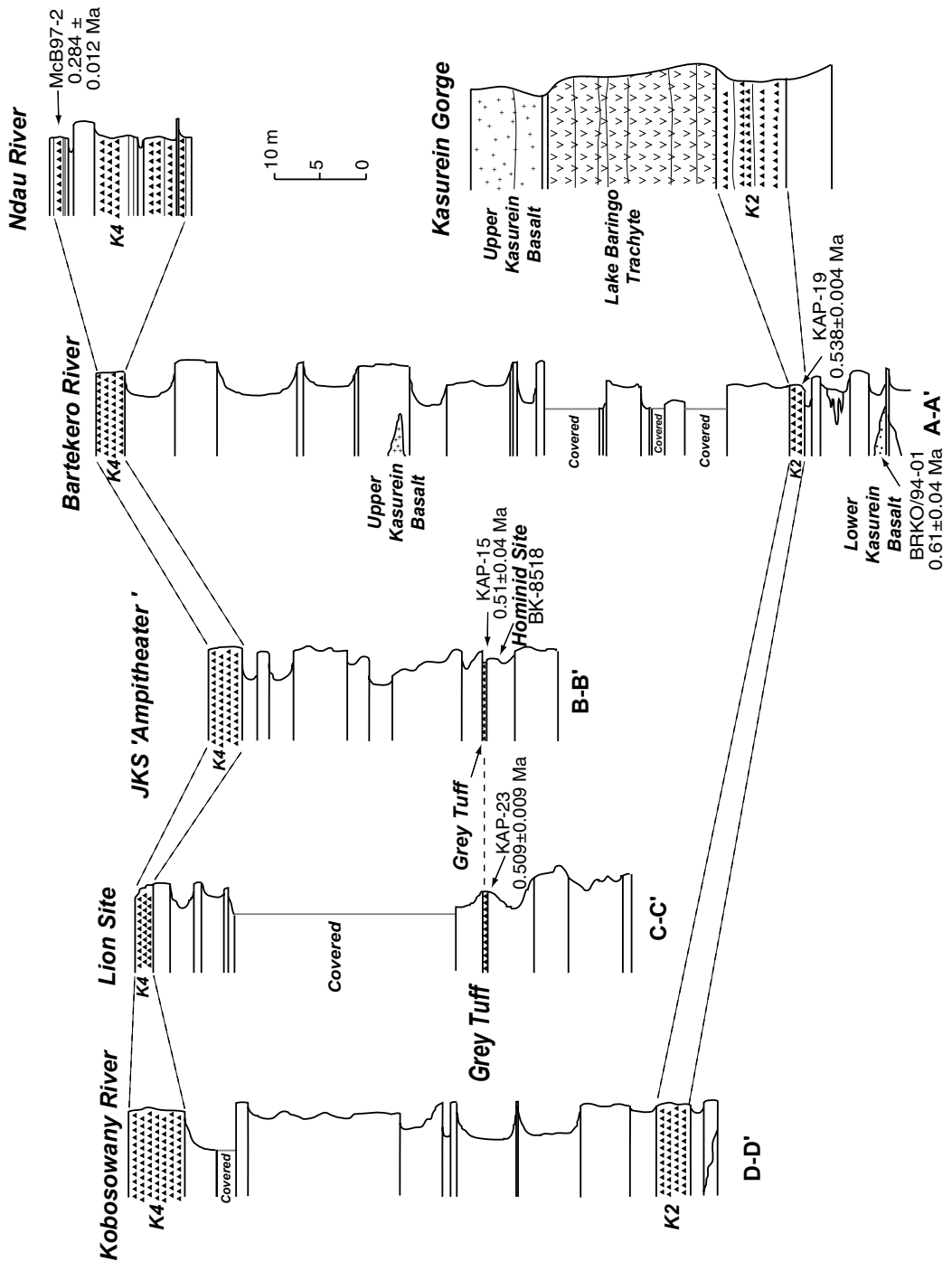

Figure 3. Measured stratigraphic sections within the Kapthurin Formation.

The Bedded Tuff (K4) probably correlates north of the study area with the lower part of the Kampi-ya-Samaki Beds (Martyn, 1969) exposed as horizontally bedded tuffs near the villages of Kampi ya Samaki and Loruk (Figure 1). Bishop *et al.* (1969) describe a section approximately 4 m thick about 2 km west of the village of Kampi ya Samaki, where the Kampi-ya-Samaki Beds overlie ''torrent washes'' resembling sediments of the Kapthurin Formation. Farther north near Loruk, the Kampi-ya-Samaki Beds lie on upfaulted blocks of Lake Baringo Trachyte. Bishop *et al.* (1969) recognize two units of the Kampi-ya-Samaki Beds, a lower, thinly bedded buff-colored tuffaceous siltstone, and an upper coarse pumiceous tuff that is interbedded with weathered siltstone. Two previous K–Ar ages of $0{\cdot}237 \pm 0{\cdot}118$ and $0{\cdot}228 \pm 0{\cdot}076$ Ma on upper Kampi-ya-Samaki Beds from near the village of Kampi ya Samaki have been reported (J. A. Miller cited in Tallon, 1976). Geochemical analysis (Tryon & McBrearty, 2002) confirms the view of Bishop *et al.* (1969) and Tallon (1976) that the lower Kampi-ya-Samaki Beds are the lateral equivalent of the Kapthurin Formation Bedded Tuff (K4) exposed throughout most of the study area. The upper, pumiceous Kampi-ya-Samaki Beds have not been observed in the Kapthurin Formation except possibly for a pumiceous tuff occurring along the northern bank of the Ndau River, as discussed below.

Our recent field investigations and new radiometric ages serve to clarify the stratigraphic relationships among several volcanic units in the Kapthurin Formation that were previously misunderstood (Figure 2). Martyn (1969) believed that all lavas of the Chemakilani Group, including both the Lower and Upper Kasurein Basalts, underlay the Kapthurin Formation. Tallon (1978) found that the Upper Kasurein Basalt was intercalated within sediments of the Kapthurin Formation, but he followed Martyn (1969) in placing the Lower Kasurein Basalt below the Kapthurin Formation Lower Silts and Gravels member (K1). Cornelissen *et al.* (1990) placed both the Upper and Lower Kasurein Basalts, as well as sediments of the lacustrine facies of the Middle Silts and Gravels member (K3′) in a separate formation, the Kwaibus Formation, which they believed to lie stratigraphically between the Kapthurin Formation and the underlying Chemeron Formation. This interpretation was found to be in error by McBrearty *et al.* (1996; McBrearty, 1999), who confirmed the stratigraphic position of lacustrine facies (K3′) sediments above the Pumice Tuff (K2) and below the Bedded Tuff (K4) (see Figure 3). We also report that the Lower Kasurein Basalt is actually intercalated within the siltstones and claystones of K1′, as described below.

Stone artefacts and fossil flora and fauna are reported from more than 40 archaeological and paleontological localities distributed through the Kapthurin Formation (Leakey *et al.*, 1969; Van Noten *et al.*, 1983, 1987*a*, 1987*b*; Cornelissen *et al.*, 1990; McBrearty *et al.*, 1996; McBrearty, 1999), and hominid remains (KNM-BK-63-67 and 8518) have been found in K3 at localities immediately below the Grey Tuff (Leakey *et al.*, 1969; Van Noten, 1982; Van Noten & Wood, 1985; Wood & Van Noten, 1986).

$^{40}Ar/^{39}Ar$ methodology

Two variants of the $^{40}Ar/^{39}Ar$ geochronological technique were utilized to date volcanic materials in this study: (1) single-crystal total-fusion (SCTF) of individual or small populations of phenocrysts in a single step, using either a focused CO_2 or Ar-ion laser as the heat source (Deino & Potts, 1990; Deino *et al.*, 1990), and (2) laser incremental heating (LIH) experiments on multi-grain samples using a uniform-energy, 6×6 mm CO_2 laser beam (Sharp & Deino, 1996).

The SCTF method was applied to anorthoclase phenocrysts from seven tuff samples, and plagioclase from a mafic tuff which did not contain a K-feldspar. Anorthoclase phenocrysts were analyzed as individual grains, while the plagioclase phenocrysts, due to their lower K content, were dated either as single grains or as aggregates of five grains in order to obtain enough gas for accurate mass spectrometric analysis.

The SCTF results are provided in Table 1, and displayed as age-probability density plots in Figures 4–6. All SCTF samples show quasi-symmetrical, unimodal age distributions, indicating that the anorthoclase phenocrysts belong to a single juvenile population. The proportion of radiogenic to atmospheric ^{40}Ar (%^{40}Ar*), usually between 60 and 90%, is reasonable for unaltered anorthoclase of this age. A few grains yielded significantly lower radiogenic argon than this norm, but exclusion of these analyses produced insignificant differences in the weighted mean sample ages and so were retained in the dataset. These characteristics of the analytical data suggest that the ^{40}Ar/^{39}Ar age determinations on the anorthoclase phenocrysts provide a geologically accurate assessment of eruption ages. Although the Ca/K ratio of some of the anorthoclase samples varied by more than an order of magnitude, this likely reflects variations in magma chamber crystallization chemistry rather than evidence of contamination. While the age-probability distributions for the plagioclase are also quasi-symmetric and unimodal, the scatter of the analyses is so great due to the low K content of the material that the ages are of little use.

Phenocrysts and/or groundmass from six volcanic flows were analyzed using the LIH technique. These include two samples from the Lake Baringo Trachyte, one from the Lower Kasurein Basalt, and three from the Upper Kasurein Basalt (Table 2; Figures 7 and 8). In some cases groundmass samples were treated experimentally with dilute HF or HNO_3 in an effort to remove fine-grained alteration products or residual glass, as described below.

^{40}Ar/^{39}Ar results

The new ^{40}Ar/^{39}Ar ages presented here provide an improved age estimate for the oldest rocks within the Kapthurin Formation. Sample BRKO/94-1 is from the outflow portion of a mafic intrusive neck and flow complex (Lower Kasurein Basalt) contemporaneous with deposition of the stratigraphically lowest exposures of the lacustrine facies of the Lower Silts and Gravels Member (K1′) along the lower Bartekero River (Figure 1). The complex is marked within the brown siltstones and clays of K1′ by a conformable basaltic tephra blanket that can be traced westward from the vent for tens of meters in a channel cut.

LIH experiments on plagioclase phenocrysts from BRKO/94-1 (Figure 7) resulted in a highly discordant spectrum (21256-01). In a second experiment, the groundmass was treated with dilute hydrofluoric acid (7%) for 3 min to remove fine-grained material such as clay and zeolites (21259-01); while in a control experiment the groundmass was analyzed without treatment (21261-01). Analysis of the untreated groundmass gave discordant apparent age spectrum, although the degree of discordancy was minor. Analysis of the acid-treated sample resulted in a very broad plateau, encompassing about 96% of the total ^{39}Ar release, with a plateau age of $0{\cdot}61 \pm 0{\cdot}04$ Ma (see Fleck *et al.*, 1977 for plateau criteria).

Our age for the Lower Kasurein Basalt is significantly younger than four previous K–Ar ages reported by Cornelissen *et al.* (1990), which range from 1·5–1·1 Ma, with a "best guess" of 1·2 Ma. We consider our ^{40}Ar/^{39}Ar plateau age more accurate,

Table 1 $^{40}Ar/^{39}Ar$ total-fusion (SCTF) analytical data

Lab ID#	Ca/K	$^{36}Ar/^{39}Ar$	$^{40}Ar^{\star}/^{39}Ar$	Mol $^{39}Ar \times 10^{15}$	$\%^{40}Ar^{\star}$	Age (Ma) ± 1 σ
Grey Tuff; Sample KAP-15 (anorthoclase; $\mathcal{J}=3{\cdot}494 \times 10^{-4} \pm 2 \times 10^{-6}$)						
4124-01	0·1758	0·00059	0·779	2·1	82·3	0·491 ± 0·056
4124-02	0·3637	0·00077	0·884	1·1	80·5	0·557 ± 0·092
4124-03	n.d.	0·00064	0·856	0·7	81·9	0·539 ± 0·134
4124-04	n.d.	0·00086	0·807	1·5	76·1	0·508 ± 0·086
4124-05	n.d.	0·00065	0·861	0·9	81·7	0·542 ± 0·102
4124-06	n.d.	0·00100	0·759	1·1	71·9	0·478 ± 0·084
			Weighted average, 1 σ error without error in $\mathcal{J}$=			0·51 ± 0·04
				1 σ error with error in $\mathcal{J}$=		0·04
Grey Tuff; Sample KAP-23 (anorthoclase; $\mathcal{J}=1{\cdot}377 \times 10^{-4} \pm 8 \times 10^{-7}$)						
20559-02	0·0065	0·00036	2·210	1·2	95·4	0·549 ± 0·050
20559-03	0·0439	0·00024	2·201	1·9	96·9	0·547 ± 0·033
20559-04	0·0082	0·00144	2·036	1·4	82·7	0·505 ± 0·044
20559-05	0·0206	0·00406	1·916	0·9	61·5	0·476 ± 0·067
20559-06	0·0182	0·00255	2·008	1·4	72·7	0·498 ± 0·043
20559-07	0·0175	0·00275	2·344	1·6	74·2	0·582 ± 0·039
20559-08	0·0362	0·00147	2·037	1·4	82·5	0·506 ± 0·043
20559-09	0·0539	0·00216	2·153	1·1	77·2	0·535 ± 0·054
20559-10	0·0877	0·00271	2·281	1·0	74·1	0·567 ± 0·061
20559/2-02	0·1066	0·00522	2·065	0·4	57·3	0·512 ± 0·119
20559/2-03	0·3257	0·00558	2·161	1·3	56·9	0·537 ± 0·036
20559/2-04	0·1348	0·00351	1·857	1·1	64·3	0·461 ± 0·040
20559/2-05	0·5455	0·00362	1·887	1·1	64·3	0·469 ± 0·043
20559/2-06	0·0713	0·00889	1·883	0·6	41·8	0·467 ± 0·075
20559/2-07	0·0802	0·00148	2·131	2·0	83·1	0·529 ± 0·022
20559/2-08	0·3294	0·00310	2·015	1·1	69·1	0·500 ± 0·039
20559/2-09	0·0633	0·00199	2·015	2·3	77·5	0·500 ± 0·019
20559/2-10	0·1795	0·00285	1·793	1·4	68·2	0·446 ± 0·028
			Weighted average, 1 σ error without error in $\mathcal{J}$=			0·509 ± 0·009
				1 σ error with error in $\mathcal{J}$=		0·009
Pumice Tuff; Sample KAP-19 (anorthoclase; $\mathcal{J}=1{\cdot}390 \times 10^{-4} \pm 8 \times 10^{-7}$)						
20551/2-01	0·0298	0·00336	2·123	3·9	68·2	0·532 ± 0·012
20551/2-02	0·0286	0·00392	2·123	4·4	64·7	0·532 ± 0·012
20551/2-03	0·0268	0·00410	2·039	3·5	62·7	0·511 ± 0·014
20551/2-04	0·0205	0·00435	2·121	3·1	62·3	0·532 ± 0·016
20551/2-05	0·0138	0·00142	2·094	4·4	83·3	0·525 ± 0·009
20551/2-06	0·0224	0·00475	2·213	2·5	61·2	0·555 ± 0·017
20551/2-07	0·0186	0·00089	2·165	9·6	89·2	0·543 ± 0·005
20551/2-08	0·0118	0·00189	2·178	4·7	79·6	0·547 ± 0·008
20551/2-09	0·0301	0·01163	2·190	1·0	38·9	0·550 ± 0·041
20551/2-11	0·0433	0·00105	2·169	2·8	87·5	0·545 ± 0·014
20551/2-12	0·0221	0·00220	2·112	5·2	76·5	0·529 ± 0·008
			Weighted average, 1 σ error without error in $\mathcal{J}$=			0·538 ± 0·003
				1 σ error with error in $\mathcal{J}$=		0·004
Pumice Tuff; Sample KAP-21 (anorthoclase; $\mathcal{J}=1{\cdot}376 \times 10^{-4} \pm 8 \times 10^{-7}$)						
20556/2-01	0·0802	0·00453	2·217	5·0	62·4	0·551 ± 0·009
20556/2-02	0·0245	0·00573	2·230	3·6	56·9	0·554 ± 0·011
20556/2-03	0·0513	0·00357	2·199	4·6	67·6	0·546 ± 0·010
20556/2-05	0·0352	0·00325	2·215	3·6	69·8	0·550 ± 0·012
20556/2-06	0·0475	0·10105	2·192	1·9	6·8	0·545 ± 0·067
			Weighted average, 1 σ error without error in $\mathcal{J}$=			0·548 ± 0·003
				1 σ error with error in $\mathcal{J}$=		0·004

Table 1 *Continued*

Lab ID#	Ca/K	^{36}Ar/^{39}Ar	^{40}Ar*/^{39}Ar	Mol ^{39}Ar × 10^{15}	%^{40}Ar*	Age (Ma) ± 1 σ
Pumice Tuff; Sample KAP-22 (anorthoclase; $\mathcal{J}$=1·374 × 10^{-4} ± 8 × 10^{-7})						
20557/2-01	0·0433	0·00105	2·169	2·8	87·5	0·538 ± 0·014
20557/2-02	0·2017	0·02131	2·188	2·6	25·8	0·543 ± 0·020
20557/2-03	0·0016	0·04400	2·222	12·8	14·6	0·551 ± 0·016
20557/2-04	0·0509	0·00136	2·176	4·2	84·4	0·540 ± 0·009
20557/2-06	0·1041	0·00088	2·126	4·4	89·3	0·527 ± 0·009
20557/2-07	0·0433	0·00105	2·169	2·8	87·5	0·538 ± 0·014
20557/2-09	0·0201	0·00174	2·196	14·7	81·0	0·545 ± 0·004
			Weighted average, 1 σ error without error in $\mathcal{J}$=			0·542 ± 0·002
				1 σ error with error in $\mathcal{J}$=		0·004
Bedded Tuff; Sample S15-1 (plagioclase; one grain per a; $\mathcal{J}$=1·300 × 10^{-4} ± 6 × 10^{-7})						
21280B-01	23·6	0·075	7·841	0·0033	26·7	1·84 ± 2·35
21280B-02	52·0	0·292	− 6·110	0·0009	− 7·7	− 1·43 ± 12·82
21280B-05	51·0	0·064	8·410	0·0028	33·1	1·97 ± 2·56
21280B-07	34·9	0·059	9·279	0·0053	36·4	2·18 ± 1·30
21281B-01	54·0	0·122	− 2·040	0·0117	− 6·3	− 0·48 ± 0·83
21281B-02	24·6	0·077	− 5·242	0·0058	− 31·4	− 1·23 ± 1·43
21281B-03	54·7	0·225	− 8·751	0·0045	− 15·4	− 2·05 ± 2·44
21281B-04	26·9	0·039	0·644	0·0074	5·8	0·15 ± 1·05
21281B-05	39·2	0·178	− 1·327	0·0091	− 2·6	− 0·31 ± 1·10
21281B-06	48·0	0·051	1·104	0·0238	7·7	0·26 ± 0·35
21281B-08	56·9	0·121	2·869	0·0112	7·8	0·67 ± 0·83
21281B-09	50·2	0·201	0·849	0·0079	1·4	0·20 ± 1·39
21281B-10	31·4	0·006	5·865	0·0175	91·0	1·38 ± 0·46
21281B-11	61·3	0·251	2·840	0·0040	3·7	0·67 ± 2·91
21281B-12	67·4	0·148	− 6·646	0·0033	− 18·7	− 1·56 ± 2·81
21281B-15	48·3	0·018	1·463	0·0119	29·2	0·34 ± 0·65
21281B-16	58·1	0·100	− 0·377	0·0057	− 1·4	− 0·09 ± 1·92
21281B-17	50·2	0·144	− 11·555	0·0068	− 38·8	− 2·71 ± 1·62
21281B-18	26·5	0·058	− 7·098	0·0094	− 77·8	− 1·67 ± 0·80
21281B-19	23·3	0·178	− 6·939	0·0062	− 15·4	− 1·63 ± 1·51
21281B-20	41·4	0·079	9·401	0·0052	29·9	2·20 ± 1·65
21281B-21	39·2	0·240	7·197	0·0084	9·3	1·69 ± 1·40
21281B-23	27·8	0·136	1·782	0·0082	4·3	0·42 ± 1·11
21281B-24	38·1	0·472	4·371	0·0044	3·0	1·03 ± 3·98
21281B-25	24·4	0·057	− 0·997	0·0125	− 6·7	− 0·23 ± 0·64
21281B-26	39·5	0·165	4·209	0·0094	8·1	0·99 ± 1·04
21281B-27	42·9	0·195	− 2·860	0·0073	− 5·3	− 0·67 ± 1·41
21281B-28	34·7	0·033	3·375	0·0133	28·9	0·79 ± 0·58
21281B-29	51·3	0·147	5·617	0·0064	11·8	1·32 ± 1·47
21281B-30	43·5	0·235	11·526	0·0052	14·4	2·70 ± 2·29
			Weighted average, 1 σ error without error in $\mathcal{J}$=			0·34 ± 0·24
				1 σ error with error in $\mathcal{J}$=		0·24
Omitted:						
21280B-08	34·0	0·169	47·797	0·0027	49·2	11·18 ± 4·38
21281B-13	24·3	0·010	112·358	0·0092	98·2	26·17 ± 1·35
Bedded Tuff; Sample S15-1 (plagioclase; five grains per analysis; $\mathcal{J}$=1·300 × 10^{-4} ± 6 × 10^{-7})						
21281B-31	48·7	0·020	0·804	0·025	17·3	0·19 ± 0·28
21281B-32	43·7	0·046	3·125	0·034	20·6	0·73 ± 0·21
21281B-33	43·4	0·046	1·225	0·026	9·3	0·29 ± 0·27
21281B-34	43·8	0·136	1·042	0·022	2·6	0·24 ± 0·42
21281B-35	41·0	0·073	1·966	0·025	8·9	0·46 ± 0·30
21281B-36	47·9	0·067	5·673	0·019	23·9	1·33 ± 0·40
			Weighted average, 1 σ error without error in $\mathcal{J}$=			0·52 ± 0·19
				1 σ error with error in $\mathcal{J}$=		0·19

Table 1 *Continued*

Lab ID#	Ca/K	$^{36}Ar/^{39}Ar$	$^{40}Ar^{\star}/^{39}Ar$	Mol $^{39}Ar \times 10^{15}$	$\%^{40}Ar^{\star}$	Age (Ma) ± 1 σ
Bedded Tuff; Sample MCB97-2 (anorthoclase; $\mathcal{J}=1{\cdot}301 \times 10^{-4} \pm 6 \times 10^{-7}$)						
21287-01	0·1904	0·00467	1·367	1·2	49·9	0·319 ± 0·043
21287-03	0·1639	0·00559	1·127	1·9	40·7	0·263 ± 0·028
21287-04	0·2030	0·00863	1·151	1·7	31·2	0·268 ± 0·059
21287-05	0·1852	0·00792	1·108	1·1	32·2	0·258 ± 0·076
21287-06	0·1822	0·00373	1·052	1·6	49·0	0·244 ± 0·020
21287-07	0·1850	0·01296	0·869	3·3	18·5	0·203 ± 0·049
21287-08	0·2181	0·00177	1·195	1·1	69·9	0·279 ± 0·018
21287-09	0·2333	0·00293	1·117	0·7	56·6	0·260 ± 0·037
21287-10	0·1752	0·00334	1·304	1·4	57·1	0·304 ± 0·026
			Weighted average, 1 σ error without error in $\mathcal{J}$=			0·271 ± 0·013
				1 σ error with error in $\mathcal{J}$=		0·013
Omitted:						
21287-02	0·2062	0·01539	1·762	2·9	28·0	0·411 ± 0·097
Bedded Tuff; Sample MCB97-2p (anorthoclase; $\mathcal{J}=1{\cdot}301 \times 10^{-4} \pm 6 \times 10^{-7}$)						
21286-01	0·2155	0·00117	1·262	1·6	79·0	0·293 ± 0·012
21286-02	0·4530	0·00533	1·157	3·0	42·6	0·270 ± 0·021
21286-03	0·1603	0·00835	1·322	8·1	35·0	0·308 ± 0·015
21286-04	0·2013	0·00495	1·270	0·8	46·6	0·296 ± 0·063
21286-05	0·2700	0·00379	0·948	0·4	46·1	0·221 ± 0·081
21286-06	0·2324	0·00154	0·957	0·5	68·2	0·223 ± 0·030
21286-07	0·1872	0·00242	1·593	0·9	69·3	0·371 ± 0·041
21286-08	0·2008	0·00206	1·310	0·7	68·6	0·306 ± 0·036
21286-09	0·4667	0·00298	1·448	0·8	62·7	0·338 ± 0·048
21286-10	0·2610	0·00034	1·198	0·7	93·0	0·279 ± 0·016
21286-11	0·1825	0·00259	1·053	0·7	58·2	0·246 ± 0·035
21286-12	0·1615	0·00137	1·439	0·4	78·3	0·336 ± 0·067
			Weighted average, 1 σ error without error in $\mathcal{J}$=			0·291 ± 0·010
				1 σ error with error in $\mathcal{J}$=		0·011
Kampi-ya-Samaki Beds; Sample CYS97-1 (anorthoclase; $\mathcal{J}=1{\cdot}361 \times 10^{-4} \pm 3 \times 10^{-7}$)						
21042-01	0·1068	0·00287	0·998	9·69	54·2	0·246 ± 0·003
21042-02	0·1279	0·00605	0·959	2·05	35·0	0·236 ± 0·012
21042-03	0·0412	0·01457	0·970	4·29	18·4	0·239 ± 0·011
21042-04	0·0675	0·00392	0·925	5·44	44·4	0·227 ± 0·005
21042-06	0·0700	0·00164	0·930	7·99	65·9	0·228 ± 0·003
21042-08	0·0376	0·00201	0·912	9·19	60·6	0·224 ± 0·003
21042-09	0·0487	0·00311	0·985	6·30	51·8	0·242 ± 0·005
21042C-01	n.d.	0·00027	0·945	4·80	92·2	0·233 ± 0·004
21042C-02	n.d.	0·00074	1·033	1·82	82·6	0·254 ± 0·010
21044B-02	0·1059	0·00029	0·950	1·70	92·0	0·234 ± 0·005
21044B-03	0·0259	0·00038	0·930	1·98	89·3	0·228 ± 0·005
21044B-04	0·0243	0·00074	0·986	1·80	82·0	0·242 ± 0·005
21044B-05	0·1126	0·00330	0·949	1·11	49·5	0·234 ± 0·009
21044B-06	0·0877	0·00105	0·912	1·26	74·9	0·223 ± 0·007
21044B-07	0·0454	0·00050	0·937	2·14	86·6	0·230 ± 0·005
21044B-08	0·0439	0·00731	1·007	2·24	31·8	0·248 ± 0·007
21044C-01	0·0398	0·00026	0·961	7·73	92·7	0·236 ± 0·003
21044C-02	0·2614	0·00113	0·983	4·03	75·2	0·242 ± 0·005
21044C-03	0·0299	0·00068	0·965	6·54	82·9	0·237 ± 0·003
			Weighted average, 1 σ error without error in $\mathcal{J}$=			0·2346 ± 0·0019
				1 σ error with error in $\mathcal{J}$=		0·002

Table 1 *Continued*

Lab ID#	Ca/K	^{36}Ar/^{39}Ar	^{40}Ar*/^{39}Ar	Mol ^{39}Ar × 10^{15}	%^{40}Ar*	Age (Ma) ± 1 σ
Omitted (^{39}Ar<1 × 10^{-15} mol):						
21042-07	0·0810	0·00260	0·799	0·31	51·1	0·19 ± 0·07
21042-10	0·1795	0·06149	− 0·885	0·05	− 5·1	− 0·22 ± 0·51
21044B-01	47·5041	0·18123	− 3·803	0·01	− 7·8	− 0·93 ± 1·02
21044C-04	n.d.	0·00001	1·207	0·44	99·8	0·29 ± 0·04
21044C-05	2·9249	− 0·00077	1·305	0·13	136·1	0·32 ± 0·14

Notes: Several analyses of grains that did not fuse or only partially fused are omitted from the above table (<0·4 × 10^{-15} mol ^{39}Ar). Errors in age quoted for individual runs are 1 σ analytical uncertainty. Weighted averages are calculated using the inverse variance as the weighting factor (Taylor, 1982), while errors in the weighted averages are 1 σ standard error of the mean (Samson & Alexander, 1987). Ca/K is calculated from ^{37}Ar/^{39}Ar using a multiplier of 1·96. ^{40}Ar* refers to radiogenic argon. λ=5·543 × 10^{-10} y^{-1}. Lab ID# 4124 was irradiated in a Cd-lined container in the hydraulic rabbit facility of the Los Alamos Omega West reactor for 30 min, while all other samples were irradiated in the Cd-shielded CLICIT facility of the Oregon State University reactor for 30 min. Sanidine from the Pahranagat Tuff of Nevada (Best *et al.*, 1995) was used as the monitor for sample 4124, with an age of 22·782 Ma corresponding to an age of the Fish Canyon Tuff of 28·02 Ma. Fish Canyon Tuff sanidine (Renne *et al.*, 1998) was used as the fluence monitor ($\mathcal{J}$) for all other samples· "n.d." entries in the Ca/K column indicates that ^{37}Ar, the proxy for Ca content, was not detected. Isotopic interference corrections, for 4124: $(^{36}Ar/^{37}Ar)_{Ca}$=(2·58 ± 0·06) × 10^{-4}, $(^{39}Ar/^{37}Ar)_{Ca}$=(6·7 ± 0·3) × 10^{-4}, $(^{40}Ar/^{39}Ar)_{K}$=(8 ± 7) × 10^{-4}; for all other samples, $(^{36}Ar/^{37}Ar)_{Ca}$=(2·64 ± 0·02) × 10^{-4}, $(^{39}Ar/^{37}Ar)_{Ca}$=(6·73 ± 0·04) × 10^{-4}, $(^{40}Ar/^{39}Ar)_{K}$=(7 ± 3) × 10^{-4}.

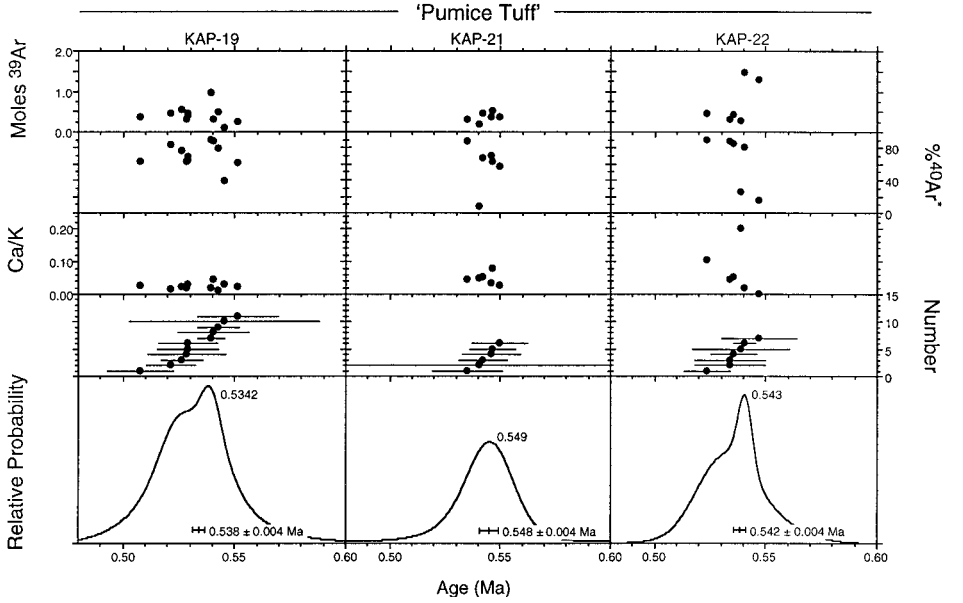

Figure 4. Age–probability density plots of SCTF results for the Pumice Tuff (K2) of the Kapthurin Formation.

because: (1) using the ^{40}Ar/^{39}Ar incremental heating method combined with multiple sample treatment methods we were able to address complications arising from sample alteration, (2) our age is consistent with available paleomagnetic data which

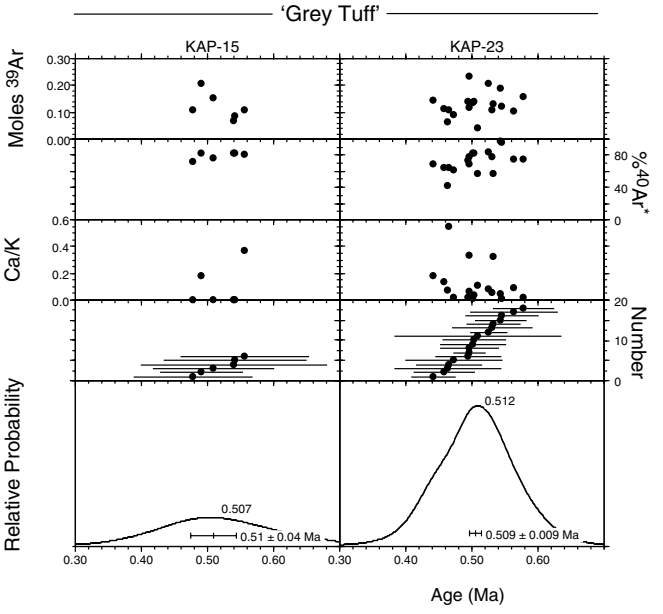

Figure 5. Age–probability density plots of SCTF results for the Grey Tuff within the Middle Silts and Gravels Member (K3) of the Kapthurin Formation.

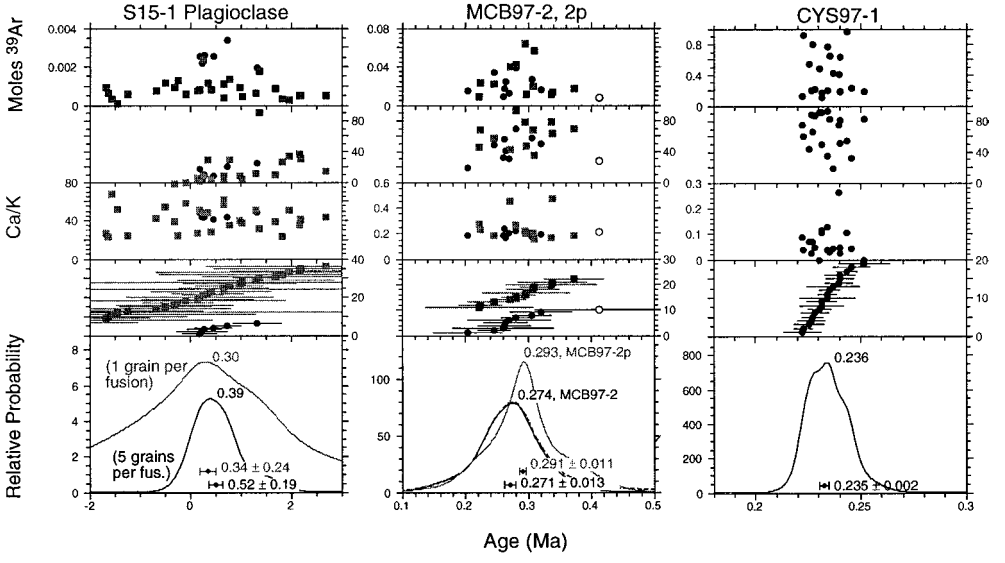

Figure 6. Age–probability density plots of SCTF results for the Bedded Tuff (K4) of the Kapthurin Formation.

indicates that the entire formation has normal polarity and probably was deposited entirely within the Brunhes epoch, and (3) there is no indication of a major unconformity with a 0·6 Ma duration within the Lower Silts and Gravels. The $^{40}Ar/^{39}Ar$ age of

Table 2 ^{40}Ar/^{39}Ar laser incremental heating (LIH) analytical data

Lab ID#	Laser power (watts)	Ca/K	^{36}Ar/^{39}Ar	^{40}Ar*/^{39}Ar	^{39}Ar (moles $\times 10^{15}$)	%^{39}Ar (of total)	%^{40}Ar*	Age (Ma $\pm$ 1 σ)
Baringo Trachyte, sample CYS-1 (Aliquot #1); trachyte matrix, $J = 1{\cdot}273 \times 10^{-4} \pm 6 \times 10^{-7}$								
†21257-01G	2·0	0·121	0·08258	2·649	1·6	2·7	9·8	0·608 ± 0·056
†21257-01H	2·5	0·087	0·01594	2·420	3·8	6·3	34·0	0·556 ± 0·014
†21257-01I	3·0	0·069	0·00410	2·367	6·4	10·7	66·2	0·544 ± 0·007
†21257-01J	3·5	0·058	0·00181	2·400	7·0	11·7	81·9	0·551 ± 0·005
†21257-01K	4·0	0·047	0·00132	2·365	6·5	11·0	85·9	0·543 ± 0·005
†21257-01L	4·5	0·046	0·00151	2·352	7·2	12·0	84·1	0·540 ± 0·005
†21257-01M	5·0	0·060	0·00173	2·370	6·0	10·1	82·3	0·544 ± 0·006
†21257-01N	6·0	0·110	0·00202	2·375	6·9	11·7	80·0	0·545 ± 0·005
†21257-01O	7·0	0·293	0·00201	2·363	4·8	8·0	80·2	0·543 ± 0·006
21257-01P	8·0	0·496	0·00217	2·255	2·3	3·9	78·4	0·518 ± 0·011
21257-01Q	10·0	1·153	0·00222	2·363	1·9	3·2	79·5	0·543 ± 0·013
21257-01R	15·0	2·287	0·00282	2·289	2·4	3·9	75·6	0·526 ± 0·011
21257-01S	22·0	2·173	0·00309	2·264	1·9	3·2	73·3	0·520 ± 0·013
						Plateau age=		0·545 ± 0·003
						Integrated age=		0·544 ± 0·004
Baringo Trachyte, sample CYS-1 (Aliquot #2); trachyte matrix, $J = 1{\cdot}273 \times 10^{-4} \pm 6 \times 10^{-7}$								
21257-02G	2·0	0·160	0·18968	3·127	1·4	1·8	5·3	0·718 ± 0·113
21257-02H	2·5	0·113	0·06054	2·956	3·4	4·5	14·2	0·679 ± 0·037
21257-02I	3·0	0·081	0·02016	2·585	5·3	7·1	30·3	0·594 ± 0·015
21257-02J	3·5	0·063	0·00754	2·505	6·3	8·4	53·0	0·575 ± 0·008
21257-02K	4·0	0·056	0·00375	2·460	6·6	8·8	69·0	0·565 ± 0·006
21257-02L	4·5	0·057	0·00285	2·394	6·8	9·1	74·0	0·550 ± 0·005
21257-02M	5·0	0·061	0·00244	2·463	7·9	10·6	77·4	0·566 ± 0·005
21257-02N	6·0	0·078	0·00207	2·557	10·3	13·8	80·8	0·587 ± 0·005
21257-02O	7·0	0·137	0·00186	2·609	8·2	10·9	82·8	0·599 ± 0·005
21257-02P	8·0	0·317	0·00199	2·779	5·9	7·8	82·9	0·638 ± 0·006
21257-02Q	10·0	0·590	0·00217	2·865	4·1	5·5	82·3	0·658 ± 0·007
21257-02R	15·0	1·360	0·00303	3·064	4·9	6·5	78·5	0·704 ± 0·007
21257-02S	22·0	1·834	0·00355	3·535	2·9	3·9	78·4	0·811 ± 0·010
						Integrated age=		0·611 ± 0·004
Baringo Trachyte, sample MGRD-7 (Aliquot #1); anorthoclase phenocrysts; $J = 1{\cdot}273 \times 10^{-4} \pm 6 \times 10^{-7}$								
21258-01G	2·0	0·060	0·01123	6·810	1·5	2·7	67·2	1·56 ± 0·02
21258-01H	2·5	0·058	0·00868	6·497	3·2	5·7	71·7	1·49 ± 0·01
21258-01I	3·0	0·052	0·00922	5·796	3·8	6·9	68·0	1·33 ± 0·01
21258-01J	3·5	0·060	0·00565	6·521	4·1	7·3	79·7	1·50 ± 0·01
21258-01K	4·0	0·058	0·00495	6·324	3·8	6·9	81·2	1·45 ± 0·01
21258-01L	4·5	0·064	0·00619	6·790	3·9	7·0	78·8	1·56 ± 0·01
21258-01M	5·0	0·065	0·00740	8·339	4·4	8·0	79·2	1·91 ± 0·01
21258-01N	6·0	0·044	0·00815	11·166	6·0	10·8	82·3	2·56 ± 0·02
21258-01O	7·0	0·045	0·01155	23·081	6·2	11·2	87·1	5·29 ± 0·03
21258-01P	8·0	0·045	0·01563	29·138	5·7	10·3	86·3	6·68 ± 0·04
21258-01Q	10·0	0·050	0·02057	46·889	5·7	10·3	88·5	10·74 ± 0·06
21258-01R	15·0	0·058	0·03061	32·724	3·5	6·4	78·4	7·50 ± 0·05
21258-01S	22·0	0·042	0·04215	12·380	1·7	3·0	49·9	2·84 ± 0·04
						Integrated age=		4·06 ± 0·02
Baringo Trachyte, sample MGRD-7 (Aliquot #2); anorthoclase phenocrysts; $J = 1{\cdot}273 \times 10^{-4} \pm 6 \times 10^{-7}$								
21258-02G	2·0	0·080	0·02630	11·139	1·4	2·8	58·9	2·56 ± 0·03
21258-02H	2·5	0·073	0·01212	10·322	2·8	5·7	74·3	2·37 ± 0·02
21258-02I	3·0	0·068	0·00751	8·655	3·9	8·0	79·6	1·99 ± 0·01
21258-02J	3·5	0·075	0·00630	8·898	3·6	7·4	82·7	2·04 ± 0·01
21258-02K	4·0	0·069	0·00602	19·314	3·5	7·2	91·6	4·43 ± 0·03

Table 2 *Continued*

Lab ID#	Laser power (watts)	Ca/K	$^{36}Ar/^{39}Ar$	$^{40}Ar^{*}/^{39}Ar$	^{39}Ar (moles $\times 10^{15}$)	$\%^{39}Ar$ (of total)	$\%^{40}Ar^{*}$	Age (Ma $\pm$ 1 σ)
Baringo Trachyte, sample MGRD-7 (Aliquot #2); anorthoclase phenocrysts; $\mathcal{J}=1{\cdot}273\times10^{-4}\pm6\times10^{-7}$								
21258-02L	4·5	0·074	0·00593	38·504	3·8	7·8	95·7	8·82 ± 0·05
21258-02M	5·0	0·085	0·00754	12·694	3·6	7·4	85·1	2·91 ± 0·02
21258-02N	6·0	0·071	0·00919	14·155	4·7	9·6	83·9	3·25 ± 0·02
21258-02O	7·0	0·059	0·01738	12·509	5·1	10·5	70·9	2·87 ± 0·02
21258-02P	8·0	0·056	0·01715	11·640	4·6	9·5	69·7	2·67 ± 0·02
21258-02Q	10·0	0·059	0·02842	30·972	5·3	10·8	78·7	7·10 ± 0·04
21258-02R	15·0	0·055	0·03868	54·414	3·3	6·7	82·6	12·45 ± 0·07
21258-02S	22·0	0·050	0·03797	7·713	1·7	3·5	40·7	1·77 ± 0·03
						Integrated age=		4·11 ± 0·02
Lower Kasurein Basalt, sample BRKO/94-1; whole-rock basalt, HF treatment; $\mathcal{J}=1{\cdot}273\times10^{-4}\pm6\times10^{-7}$								
21259-01H	2·5	5·51	1·008	− 3·674	0·2	1·5	− 1·2	− 0·84 ± 0·73
21259-01I	3·0	4·47	0·571	− 2·055	0·4	2·7	− 1·2	− 0·47 ± 0·39†
†21259-01J	3·5	3·71	0·390	2·764	0·4	3·1	2·3	0·63 ± 0·27
†21259-01K	4·0	3·06	0·300	2·924	0·5	3·6	3·2	0·67 ± 0·21
†21259-01L	4·5	2·79	0·265	1·419	0·5	3·9	1·8	0·33 ± 0·19
†21259-01M	5·0	2·61	0·236	1·490	0·6	4·3	2·1	0·34 ± 0·17
†21259-01N	6·0	2·52	0·213	2·174	1·0	7·1	3·3	0·50 ± 0·13
†21259-01O	7·0	2·45	0·178	2·942	1·1	8·0	5·3	0·68 ± 0·11
†21259-01P	8·0	2·45	0·158	2·138	1·1	8·4	4·4	0·49 ± 0·10
†21259-01Q	10·0	2·67	0·132	2·560	1·6	12·0	6·2	0·59 ± 0·08
†21259-01R	12·5	3·41	0·124	2·877	2·1	15·8	7·3	0·66 ± 0·07
†21259-01S	15·0	4·47	0·116	3·001	2·7	20·2	8·1	0·69 ± 0·06
†21259-01T	25·0	12·78	0·118	2·874	1·3	9·4	7·7	0·66 ± 0·08
						Plateau age=		0·61 ± 0·04
						Integrated age=		0·55 ± 0·03
Lower Kasurein Basalt, sample BRKO/94-1; whole-rock basalt; no HF treatment; $\mathcal{J}=1{\cdot}273\times10^{-4}\pm6\times10^{-7}$								
21261-01G	2·0	5·71	0·178	1·407	0·4	1·9	2·6	0·32 ± 0·14
21261-01H	2·5	4·99	0·101	2·038	0·6	3·0	6·4	0·47 ± 0·09
21261-01I	3·0	4·33	0·077	2·177	0·9	4·3	8·8	0·50 ± 0·06
21261-01J	3·5	3·83	0·059	2·514	0·9	4·2	12·8	0·58 ± 0·06
21261-01K	4·0	3·55	0·047	2·889	0·9	4·4	17·3	0·66 ± 0·05
21261-01L	4·5	3·45	0·042	2·662	1·0	4·6	17·7	0·61 ± 0·04
21261-01M	5·0	3·25	0·036	2·208	1·1	5·2	17·3	0·51 ± 0·04
21261-01N	6·0	3·25	0·027	2·942	2·0	9·4	27·4	0·68 ± 0·03
21261-01O	7·0	2·90	0·018	2·703	2·3	10·5	33·7	0·62 ± 0·02
21261-01P	8·0	2·65	0·017	2·908	2·2	10·2	37·3	0·67 ± 0·02
21261-01Q	10·0	3·00	0·019	3·264	2·6	12·1	37·5	0·75 ± 0·02
21261-01R	15·0	6·38	0·030	3·144	4·6	21·6	26·6	0·72 ± 0·02
21261-01S	22·0	17·00	0·080	4·421	1·7	7·8	16·0	1·02 ± 0·06
						Integrated age=		0·678 ± 0·11
Lower Kasurein Basalt, sample BRKO/94-1; plagioclase phenocrysts; $\mathcal{J}=1{\cdot}273\times10^{-4}\pm6\times10^{-7}$								
21256-01B	2·0	51·7	1·890	7·31	0·09	2·8	1·3	1·7 ± 1·6
21256-01C	3·0	50·8	0·815	5·83	0·15	4·6	2·3	1·3 ± 0·6
21256-01D	4·0	49·8	0·199	11·69	0·14	4·5	16·8	2·7 ± 0·2
21256-01E	5·0	50·0	0·189	59·70	0·18	5·6	52·1	13·7 ± 0·2
21256-01F	6·0	49·0	0·231	120·25	0·25	7·6	64·0	27·4 ± 0·3
21256-01G	7·0	49·6	0·081	72·00	0·20	6·0	76·3	16·5 ± 0·2
21256-01H	8·0	51·8	0·131	61·59	0·14	4·4	62·3	14·1 ± 0·2
21256-01I	9·0	52·4	0·070	50·66	0·12	3·7	72·8	11·6 ± 0·2
21256-01J	11·0	54·0	0·110	45·49	0·38	11·4	59·4	10·4 ± 0·1
21256-01K	13·0	54·2	0·068	46·65	0·34	10·3	71·8	10·7 ± 0·1

Table 2 *Continued*

Lab ID#	Laser power (watts)	Ca/K	^{36}Ar/^{39}Ar	^{40}Ar*/^{39}Ar	^{39}Ar (moles $\times 10^{15}$)	%^{39}Ar (of total)	%^{40}Ar*	Age (Ma $\pm$ 1 σ)
Lower Kasurein Basalt, sample BRKO/94-1; plagioclase phenocrysts; $\mathcal{J}=1{\cdot}273\times10^{-4}\pm6\times10^{-7}$								
21256-01L	17·0	53·8	0·096	87·82	0·77	23·3	76·7	20·1 ± 0·1
21256-01M	25·0	62·2	0·035	16·57	0·53	16·0	67·1	3·8 ± 0·1
						Integrated age=		12·69 ± 0·09
Upper Kasurein Basalt, sample KAP-815, groundmass, no acid treatment; $\mathcal{J}=1{\cdot}309\times10^{-4}\pm7\times10^{-7}$								
†21813-01B	2	7·44	1·3734	0·932	0·2	1·5	0·2	0·2 ± 0·8
†21813-01C	3	6·14	0·6643	1·052	0·5	3·8	0·5	0·2 ± 0·4
†21813-01D	4	5·14	0·4125	2·050	0·9	6·9	1·7	0·5 ± 0·2
†21813-01E	5	4·28	0·3095	1·705	1·2	9·5	1·8	0·40 ± 0·16
†21813-01F	6	3·74	0·2379	1·963	1·5	11·8	2·7	0·46 ± 0·12
†21813-01G	7	3·20	0·1915	2·727	1·8	14·0	4·6	0·64 ± 0·10
†21813-01H	8	2·62	0·1723	2·874	1·5	11·5	5·3	0·68 ± 0·09
†21813-01I	9	2·55	0·1549	2·608	1·0	8·0	5·4	0·62 ± 0·09
†21813-01J	10	2·67	0·1360	2·175	1·4	10·5	5·1	0·51 ± 0·07
†21813-01K	12	5·32	0·1010	2·458	1·0	8·1	7·6	0·58 ± 0·06
†21813-01L	15	8·13	0·0897	2·306	0·5	4·1	8·1	0·54 ± 0·07
†21813-01M	27	23·09	0·1087	2·225	0·7	5·4	6·6	0·53 ± 0·08
21813-01N	35	24·80	0·0864	4·629	0·3	2·6	15·8	1·09 ± 0·09
21813-01O	40	21·37	0·0740	1·149	0·3	2·3	5·1	0·27 ± 0·10
						Plateau age=		0·56 ± 0·03
						Integrated age=		0·54 ± 0·04
Upper Kasurein Basalt, sample KAP-815, groundmass, nitric acid treatment; $\mathcal{J}=1{\cdot}309\times10^{-4}\pm7\times10^{-7}$								
†21812-01C	3	7·52	0·9214	1·816	0·2	1·6	0·7	0·4 ± 0·6
†21812-01D	4	5·86	0·4835	2·615	0·5	3·3	1·8	0·6 ± 0·3
†21812-01E	5	4·69	0·3282	1·263	0·7	5·1	1·3	0·30 ± 0·18
†21812-01F	6	3·90	0·2488	2·341	1·0	7·3	3·1	0·55 ± 0·13
†21812-01G	7	3·58	0·1988	2·602	1·1	7·9	4·2	0·61 ± 0·10
†21812-01H	8	3·30	0·1490	2·451	1·3	9·5	5·3	0·58 ± 0·08
†21812-01I	9	2·82	0·1162	2·261	1·5	11·2	6·2	0·53 ± 0·07
†21812-01J	10	2·51	0·0850	2·431	1·8	13·0	8·8	0·57 ± 0·05
†21812-01K	11	2·97	0·0727	2·127	1·6	11·4	9	0·50 ± 0·04
†21812-01L	15	4·51	0·0598	2·179	2·2	16·6	11·1	0·51 ± 0·03
†21812-01M	27	17·54	0·0650	2·660	1·1	8·8	12·5	0·63 ± 0·05
21812-01N	35	25·70	0·0485	3·062	0·3	2·4	18·6	0·72 ± 0·06
21812-01O	40	19·10	0·0453	2·314	0·2	1·9	15·4	0·55 ± 0·08
						Plateau age=		0·54 ± 0·02
						Integrated age=		0·55 ± 0·03
Upper Kasurein Basalt, sample KAP-815, groundmass, nitric acid treatment; $\mathcal{J}=1{\cdot}309\times10^{-4}\pm7\times10^{-7}$								
21814-01A	2	9·60	1·5584	− 3·180	0·2	1·2	− 0·7	− 0·8 ± 1·1
21814-01B	3	7·14	0·6662	− 3·212	0·6	3·1	− 1·7	− 0·8 ± 0·4
21814-01C	4	5·25	0·3248	− 1·744	1·2	6·4	− 1·9	− 0·4 ± 0·2
21814-01D	5	4·08	0·2092	− 0·756	1·8	9·2	− 1·2	− 0·18 ± 0·13
21814-01E	6	3·24	0·1455	0·245	2·5	12·4	0·6	0·06 ± 0·09
21814-01F	7	2·67	0·1012	3·038	3·0	14·7	9·2	0·72 ± 0·08
21814-01G	8	2·64	0·0863	2·660	2·3	11·3	9·5	0·63 ± 0·07
21814-01H	9	2·45	0·0696	2·541	2·3	11·1	11	0·60 ± 0·06
21814-01I	10	2·60	0·0514	2·731	2·5	11·5	15·3	0·64 ± 0·05
21814-01J	11	3·58	0·0353	3·803	1·3	6·2	27	0·90 ± 0·05
21814-01K	15	10·07	0·0348	4·154	1·1	5·3	29·6	0·98 ± 0·06
21814-01L	27	32·91	0·0610	4·400	0·6	3·1	20·7	1·04 ± 0·08
21814-01M	35	31·21	0·0446	5·332	0·4	2·3	30·7	1·26 ± 0·10
21814-01N	40	31·38	0·0535	2·838	0·4	2·1	16·2	0·67 ± 0·10
						Integrated age=		0·43 ± 0·03

Table 2 *Continued*

Lab ID#	Laser power (watts)	Ca/K	$^{36}Ar/^{39}Ar$	$^{40}Ar^{\star}/^{39}Ar$	^{39}Ar (moles $\times 10^{15}$)	$\%^{39}Ar$ (of total)	$\%^{40}Ar^{\star}$	Age (Ma $\pm$ 1 σ)
Upper Kasurein Basalt, sample KAP-815, groundmass, nitric acid treatment; $J = 1{\cdot}309 \times 10^{-4} \pm 7 \times 10^{-7}$								
†21814B-01A	2	7·02	1·7681	8·042	0·3	1·0	1·5	1·9 ± 1·3
†21814B-01B	3	5·42	0·9279	5·671	0·7	2·4	2	1·3 ± 0·6
†21814B-01C	4	4·46	0·5862	3·333	1·3	4·4	1·9	0·8 ± 0·3
†21814B-01D	5	3·48	0·3858	3·262	1·8	6·1	2·8	0·8 ± 0·2
†21814B-01E	6	3·11	0·2644	2·701	2·1	6·9	3·3	0·64 ± 0·15
†21814B-01F	8	2·77	0·1559	3·061	3·9	12·9	6·2	0·72 ± 0·08
†21814B-01G	10	2·26	0·1043	2·350	4·2	13·8	7·1	0·55 ± 0·06
†21814B-01H	12	2·44	0·0737	2·815	4·0	13·0	11·5	0·66 ± 0·04
†21814B-01I	15	3·97	0·0675	2·558	3·9	12·6	11·4	0·60 ± 0·04
†21814B-01J	18	5·05	0·0624	2·452	1·8	5·9	11·8	0·58 ± 0·04
†21814B-01K	22	6·35	0·0654	2·426	1·1	3·4	11·3	0·57 ± 0·05
†21814B-01L	27	11·04	0·0735	2·319	1·0	3·2	9·8	0·55 ± 0·06
21814B-01M	32	14·99	0·0753	2·230	1·0	3·3	9·3	0·53 ± 0·05
21814B-01N	38	20·29	0·0589	2·638	1·1	3·5	13·6	0·62 ± 0·04
21814B-01O	40	12·11	0·0661	2·868	2·4	7·7	13	0·68 ± 0·06
						Plateau age=		0·61 ± 0·03
						Integrated age=		0·67 ± 0·03
Upper Kasurein Basalt, sample KAP-815, groundmass, nitric acid treatment; $J = 1{\cdot}309 \times 10^{-4} \pm 7 \times 10^{-7}$								
†21814-02B	3	7·61	0·8881	1·524	0·4	2·1	0·6	0·4 ± 0·6
†21814-02C	4	5·98	0·4513	2·935	1·0	4·7	2·2	0·7 ± 0·3
†21814-02D	5	4·61	0·2599	3·303	1·6	7·8	4·1	0·78 ± 0·16
†21814-02E	6	3·54	0·1764	1·902	2·3	11·4	3·5	0·45 ± 0·10
†21814-02F	7	2·88	0·1216	2·745	2·9	14·1	7·1	0·65 ± 0·07
†21814-02G	8	2·56	0·0876	2·523	3·0	14·9	8·9	0·60 ± 0·05
21814-02H	9	2·36	0·0668	3·013	2·8	13·7	13·3	0·71 ± 0·05
21814-02I	10	2·37	0·0463	4·437	2·3	11·4	24·6	1·05 ± 0·04
21814-02J	11	3·63	0·0352	6·647	1·2	5·6	39·3	1·57 ± 0·04
21814-02K	15	9·13	0·0361	25·597	1·3	6·3	71·2	6·03 ± 0·05
21814-02L	27	27·91	0·0577	21·969	0·6	3·2	57·8	5·18 ± 0·11
21814-02M	35	25·79	0·0486	24·521	0·4	2·0	64·6	5·78 ± 0·10
21814-02N	40	23·18	0·0435	30·933	0·5	2·7	72	7·29 ± 0·10
						Plateau age=		0·60 ± 0·05
						Integrated age=		1·50 ± 0·03
Upper Kasurein Basalt, sample S15-3, groundmass, no acid treatment; $J = 1{\cdot}277 \times 10^{-4} \pm 1 \times 10^{-6}$								
†21269-01K	4	5·62	0·4670	2·108	0·4	1·2	1·5	0·5 ± 0·3
†21269-01L	4·5	5·23	0·3754	3·647	0·5	1·6	3·2	0·8 ± 0·2
†21269-01M	5	5·13	0·3183	2·713	0·7	2·4	2·8	0·62 ± 0·19
†21269-01N	6	4·81	0·2358	2·775	1·3	4·1	3·8	0·64 ± 0·13
†21269-01O	7	4·34	0·1908	1·805	1·7	5·4	3·1	0·41 ± 0·12
†21269-01P	8	3·85	0·1569	2·303	1·9	6·1	4·7	0·53 ± 0·09
†21269-01Q	10	3·62	0·1315	2·704	2·9	9·3	6·5	0·62 ± 0·07
†21269-01R	13	4·37	0·1234	2·186	3·9	12·6	5·7	0·50 ± 0·06
†21269-01S	17	5·31	0·0987	2·423	7·2	22·7	7·7	0·56 ± 0·05
†21269-01T	19	6·69	0·0734	2·268	7·5	23·7	9·6	0·52 ± 0·04
†21269-01U	22	15·84	0·0509	2·609	2·2	6·9	15·3	0·60 ± 0·04
21269-01V	25	19·27	0·0317	2·184	1·2	3·9	20·2	0·50 ± 0·03
						Plateau age=		0·56 ± 0·03
						Integrated age=		0·55 ± 0·02
Upper Kasurein Basalt, sample S15-3, groundmass, HF acid treatment; $J = 1{\cdot}277 \times 10^{-4} \pm 1 \times 10^{-6}$								
†21271-01B	2	5·37	0·8871	2·766	1·2	2·9	1	0·6 ± 0·5
†21271-01C	3	3·53	0·1997	2·394	3·6	9	3·9	0·55 ± 0·10

Table 2 *Continued*

Lab ID#	Laser power (watts)	Ca/K	^{36}Ar/^{39}Ar	^{40}Ar*/^{39}Ar	^{39}Ar (moles × 10^{15})	%^{39}Ar (of total)	%^{40}Ar*	Age (Ma ± 1 σ)
Upper Kasurein Basalt, sample S15-3, groundmass, HF acid treatment; $\mathcal{J}=1{\cdot}277\times10^{-4}\pm1\times10^{-6}$								
†21271-01D	4	3·07	0·1011	2·329	4·0	9·9	7·3	0·54 ± 0·05
†21271-01E	5	2·93	0·0727	2·449	4·7	11·8	10·3	0·56 ± 0·04
†21271-01F	6	2·83	0·0548	2·507	5·6	14·1	13·5	0·58 ± 0·03
†21271-01G	7	2·77	0·0471	2·259	5·6	14	14·1	0·52 ± 0·02
†21271-01H	8	2·89	0·0488	2·439	5·2	12·9	14·6	0·56 ± 0·02
†21271-01I	9	3·45	0·0455	2·398	5·3	12·9	15·2	0·55 ± 0·02
†21271-01J	11	9·16	0·0391	2·458	4·4	11	18	0·57 ± 0·02
†21271-01K	13	22·02	0·0455	2·262	0·6	1·4	15·2	0·52 ± 0·07
						Plateau age=		0·556 ± 0·009
						Integrated age=		0·556 ± 0·019
Upper Kasurein Basalt, sample S15-3, groundmass, HF acid treatment; $\mathcal{J}=1{\cdot}277\times10^{-4}\pm1\times10^{-6}$								
21272-01B	1·5	5·02	0·1183	65·695	0·5	2·8	65·4	15·02 ± 0·13
21272-01C	2	2·04	0·0349	3·258	1·4	8·2	24·1	0·75 ± 0·03
21272-01D	2·5	3·40	0·0579	2·958	1·0	5·9	14·8	0·68 ± 0·05
21272-01E	3	3·26	0·0530	2·644	1·0	6	14·5	0·61 ± 0·05
21272-01F	3·5	2·87	0·0471	2·960	1·0	6·2	17·7	0·68 ± 0·05
21272-01G	4	2·77	0·0481	2·682	1·0	6·1	16	0·62 ± 0·05
21272-01H	5	2·60	0·0440	2·629	1·6	9·9	16·9	0·60 ± 0·04
21272-01I	6	3·02	0·0439	2·482	1·8	10·8	16·2	0·57 ± 0·03
21272-01J	7	2·87	0·0358	2·239	1·6	9·8	17·6	0·51 ± 0·03
21272-01K	8	2·84	0·0336	2·146	1·3	8·1	17·9	0·49 ± 0·03
21272-01L	9	3·23	0·0365	1·845	1·1	6·1	14·8	0·42 ± 0·04
21272-01M	11	5·04	0·0409	2·217	1·1	6·2	15·7	0·51 ± 0·04
21272-01N	13	7·35	0·0387	2·238	1·1	6·2	16·7	0·51 ± 0·04
21272-01O	17	15·08	0·0384	2·079	1·1	6·1	16·2	0·48 ± 0·04
21272-01P	25	34·29	0·0604	1·721	0·2	1·5	9·4	0·40 ± 0·13
						Integrated age=		0·971 ± 0·012
Upper Kasurein Basalt, sample S15-3, groundmass, HF acid treatment; $\mathcal{J}=1{\cdot}277\times10^{-4}\pm1\times10^{-6}$								
†21272-02C	2	4·84	0·1182	3·002	0·5	2·4	7·9	0·69 ± 0·12
†21272-02D	2·5	3·71	0·0727	2·669	0·9	4·7	11·1	0·61 ± 0·07
†21272-02E	3	3·40	0·0620	2·422	0·9	5	11·7	0·56 ± 0·06
†21272-02F	3·5	3·13	0·0595	2·931	0·9	5	14·4	0·67 ± 0·06
†21272-02G	4	3·13	0·0631	2·336	0·9	5	11·2	0·54 ± 0·05
†21272-02H	5	3·28	0·0621	2·449	1·4	7·9	11·8	0·56 ± 0·05
†21272-02I	6	3·20	0·0544	2·573	1·7	9·5	13·9	0·59 ± 0·04
†21272-02J	7	3·08	0·0500	2·629	1·7	9·6	15·2	0·60 ± 0·04
†‡21272-02K	8	3·04	0·0448	2·362	1·6	9	15·2	0·54 ± 0·04
‡21272-02L	9	3·14	0·0411	2·185	1·5	8·1	15·4	0·50 ± 0·04
‡21272-02M	11	4·35	0·0421	2·130	1·6	8·9	14·8	0·49 ± 0·04
‡21272-02N	13	5·36	0·0441	2·138	1·7	8·7	14·3	0·49 ± 0·04
‡21272-02O	17	8·73	0·0434	2·276	2·5	12·8	15·4	0·52 ± 0·03
‡21272-02P	25	31·96	0·0579	2·479	0·6	3·5	13·4	0·57 ± 0·02
						Plateau age (o)=		0·58 ± 0·009
						Plateau age (°)=		0·58 ± 0·009
						Integrated age=		0·554 ± 0·012

Notes: All steps yielding less than 1% of the total ^{39}Ar released were omitted from the table· "†" or "‡" indicates steps included in apparent-age plateau· ^{40}Ar* refers to radiogenic argon· Samples were irradiated in the in-core Cd-lined CLICIT facility of the Oregon State University TRIGA reactor for 30 min. Isotopic interference corrections: $(^{36}Ar/^{37}Ar)_{Ca}=2{\cdot}72\times10^{-4}\pm1\times10^{-6}$, $(^{39}Ar/^{37}Ar)_{Ca}=7{\cdot}11\times10^{-4}\pm2\times10^{-6}$, $(^{40}Ar/^{39}Ar)_{K}=7\times10^{-4}\pm3\times10^{-4}$. $\lambda=5{\cdot}543\times10^{-10}$ y^{-1}. $\mathcal{J}$ is the neutron fluence parameter.

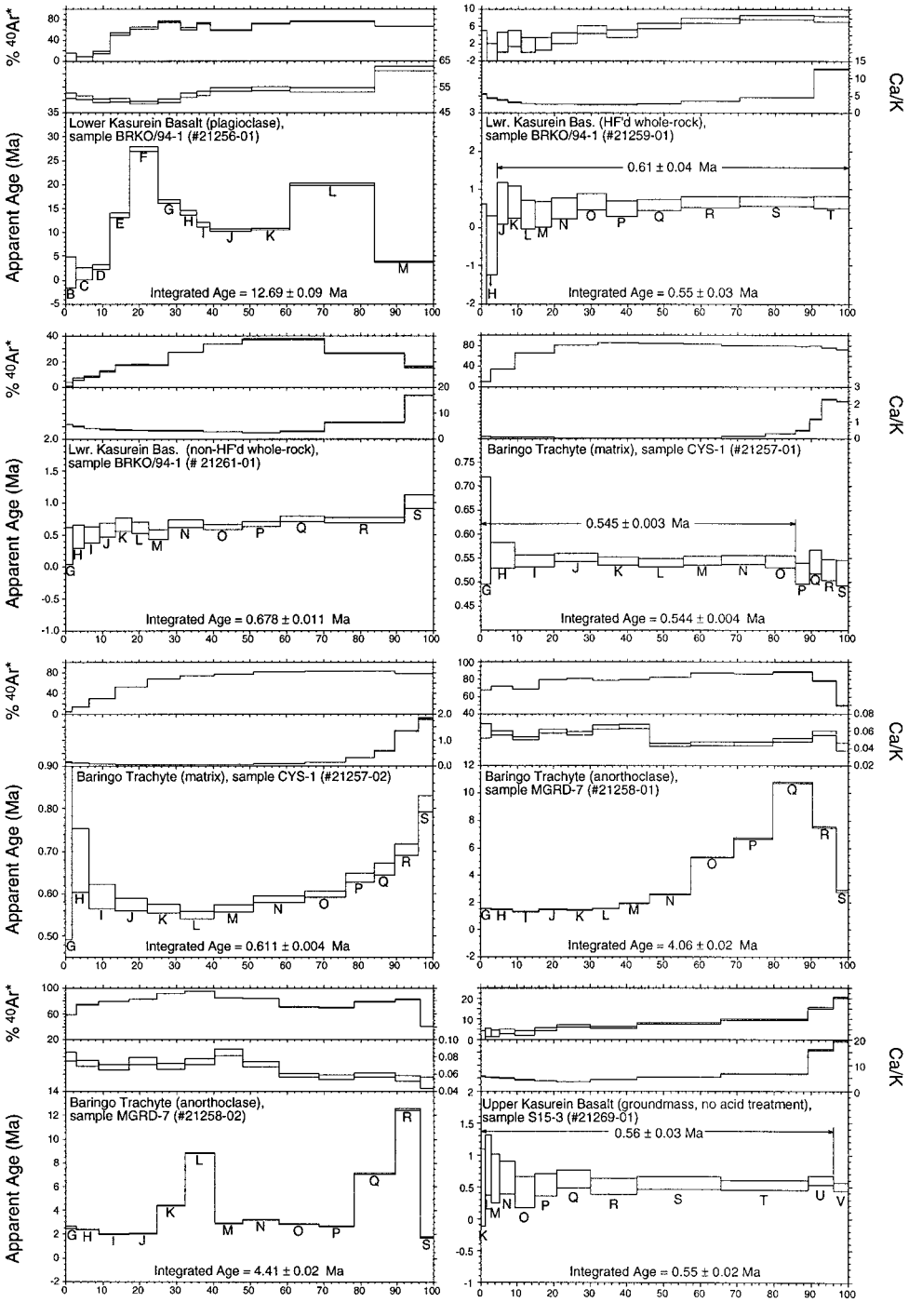
% 40Ar*
Apparent Age (Ma)
Ca/K
Lower Kasurein Basalt (plagioclase), sample BRKO/94-1 (#21256-01)
Integrated Age = 12.69 ± 0.09 Ma
Lwr. Kasurein Bas. (HF'd whole-rock), sample BRKO/94-1 (#21259-01)
0.61 ± 0.04 Ma
Integrated Age = 0.55 ± 0.03 Ma
Lwr. Kasurein Bas. (non-HF'd whole-rock), sample BRKO/94-1 (# 21261-01)
Integrated Age = 0.678 ± 0.011 Ma
Baringo Trachyte (matrix), sample CYS-1 (#21257-01)
0.545 ± 0.003 Ma
Integrated Age = 0.544 ± 0.004 Ma
Baringo Trachyte (matrix), sample CYS-1 (#21257-02)
Integrated Age = 0.611 ± 0.004 Ma
Baringo Trachyte (anorthoclase), sample MGRD-7 (#21258-01)
Integrated Age = 4.06 ± 0.02 Ma
Baringo Trachyte (anorthoclase), sample MGRD-7 (#21258-02)
Integrated Age = 4.41 ± 0.02 Ma
Upper Kasurein Basalt (groundmass, no acid treatment), sample S15-3 (#21269-01)
0.56 ± 0.03 Ma
Integrated Age = 0.55 ± 0.02 Ma
Cumulative %39Ar

0·61 ± 0·04 Ma is more consistent with the chronostratigraphy established for overlying units of the Kapthurin Formation, as discussed below. This new age for the base of the Kapthurin Formation indicates that the unconformity between the Kapthurin Formation and the underlying Chemeron Formation encompasses about 1 Ma, rather than the 0·4 Ma estimate based on prior age information.

The deposition of the Lower Silts and Gravels Member (K1) was terminated with the emplacement of the air-fall Pumice Tuff (K2). Anorthoclase phenocrysts extracted from three samples of this unit were dated; KAP-22 from the bank of the Kapthurin River, KAP-19 from the lower Bartekero River near site GnJh-57, and KAP-21 from beneath the Lake Baringo Trachyte in the Kasurein River gorge (Figure 1). The weighted-mean SCTF age of 0·542 ± 0·004 Ma for the Pumice Tuff (Figure 4) from the Kapthurin River (KAP-22) is indistinguishable at the 95% confidence level from a similar pumiceous tuff from the Bartekero River drainage dated here at 0·538 ± 0·004 Ma (KAP-19), lending support to Tallon's (1976) assessment that these beds are equivalent. A lithologically similar stratified tuff occurring immediately beneath the Lake Baringo Trachyte in the Kasurein River gorge (sample KAP-21) yielded an age of 0·548 ± 0·004 Ma, likewise indistinguishable from samples just described, indicating that this exposure is also attributable to the Pumice Tuff unit (K2). A combined weighted-mean age for the Pumice Tuff of 0·543 ± 0·004 Ma is calculated from these three samples. Our new age for the Pumice Tuff is younger than a previous K/Ar date of 0·62 ± 0·06 Ma on sanidine by Cornelissen *et al.* (1990), though statistically indistinguishable.

Our LIH apparent age results for matrix (sample CYS-1) and anorthoclase (sample MGRD-7) separates from the Lake Baringo Trachyte are quite variable (Figure 7). The anorthoclase experiments yielded highly discordant spectra with ages varying from about 1 to 12 Ma; the exact pattern of this discordance was unreproducible between replicates (21258-01, 21258-02). Integrated ages for these experiments were demonstrably too old, approximately 4·1 and 4·4 Ma. LIH experiments on Lake Baringo Trachyte matrix yielded a broad saddle-shaped spectrum (21257-02), and a nearly perfectly flat release pattern (21257-01) in two aliquots of the same material. Integrated ages of the matrix experiments are both much younger than of the anorthoclase, 0·611 ± 0·004 and 0·544 ± 0·004 Ma. These data suggest that anorthoclase phenocrysts in the Lake Baringo Trachyte bear excess Ar, and that some anorthoclase was present in 21257-02, but virtually absent from 21257-01. Given the broad plateau present in run 21257-01 on matrix material, its ultimately high (>80%) radiogenic content, uniformly low Ca/K ratio within the plateau steps, and the close agreement of plateau and integrated ages, the plateau age of 0·545 ± 0·003 Ma for this experiment is believed to reflect an accurate age for the Lake Baringo Trachyte. This result is consistent with, but more precise than, the previous K–Ar age estimate of 0·56 ± 0·04 Ma reflecting the mean of four of 11 available analytical measurements (total range 0·40 ± 0·02 to 0·84 ± 0·03 Ma; Cornelissen *et al.*, 1990).

This age is almost identical to the SCTF age obtained for the Pumice Tuff (K2) of 0·543 ± 0·004 (Figure 4), consistent with the field observations of Martyn (1969) and Tallon (1976) that the Pumice Tuff is derived from the same eruptive sequence as

Figure 7. Results of LIH analyses for the Lower Kasurein Basalt (Jl^{e}), the Lake Baringo Trachyte, and the Upper Kasurein Basalt (K3^{a}).

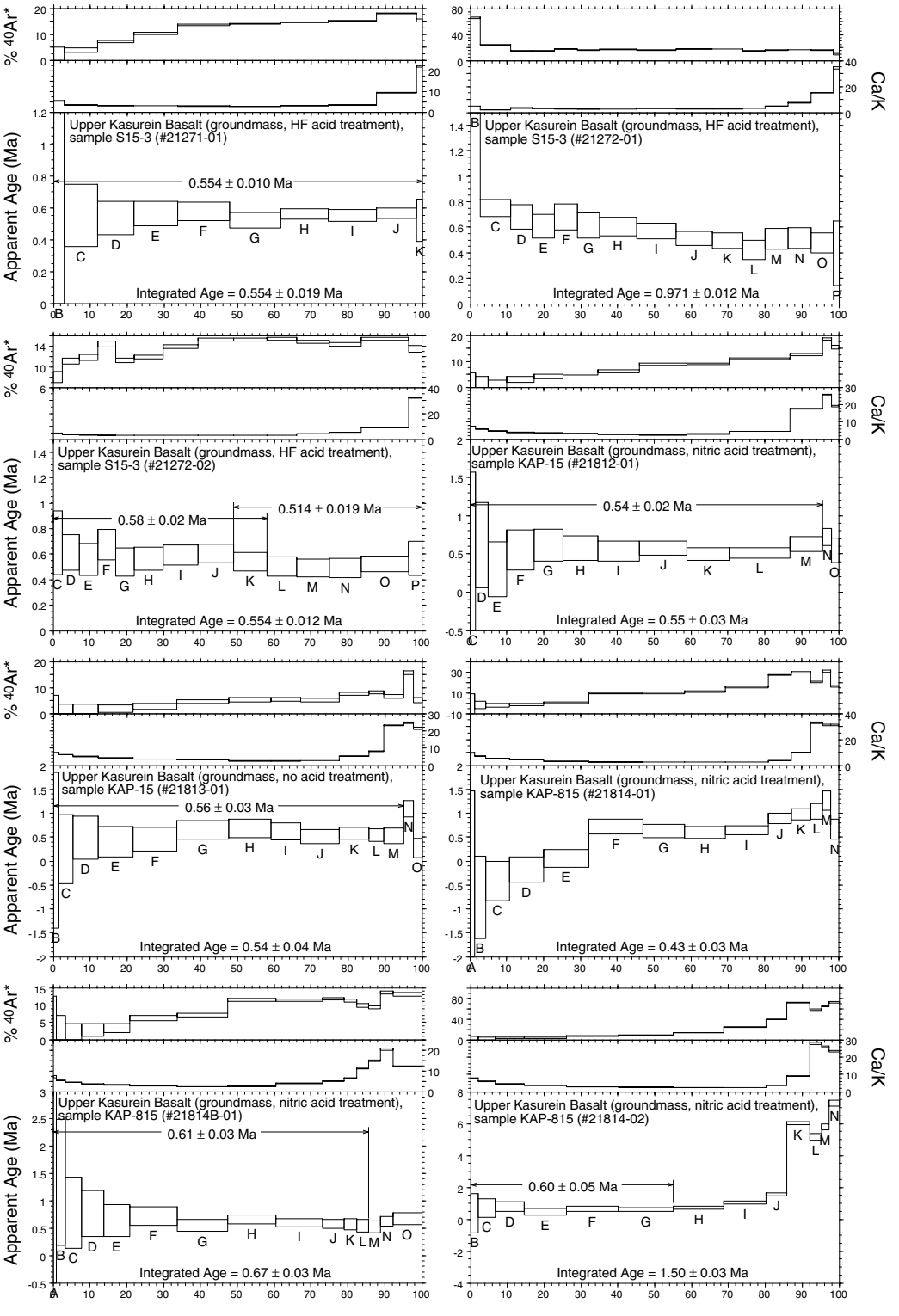
% 40Ar*
Ca/K
Apparent Age (Ma)
Upper Kasurein Basalt (groundmass, HF acid treatment), sample S15-3 (#21271-01)
0.554 ± 0.010 Ma
Integrated Age = 0.554 ± 0.019 Ma
Upper Kasurein Basalt (groundmass, HF acid treatment), sample S15-3 (#21272-01)
Integrated Age = 0.971 ± 0.012 Ma
Upper Kasurein Basalt (groundmass, HF acid treatment), sample S15-3 (#21272-02)
0.58 ± 0.02 Ma
0.514 ± 0.019 Ma
Integrated Age = 0.554 ± 0.012 Ma
Upper Kasurein Basalt (groundmass, nitric acid treatment), sample KAP-15 (#21812-01)
0.54 ± 0.02 Ma
Integrated Age = 0.55 ± 0.03 Ma
Upper Kasurein Basalt (groundmass, no acid treatment), sample KAP-15 (#21813-01)
0.56 ± 0.03 Ma
Integrated Age = 0.54 ± 0.04 Ma
Upper Kasurein Basalt (groundmass, nitric acid treatment), sample KAP-815 (#21814-01)
Integrated Age = 0.43 ± 0.03 Ma
Upper Kasurein Basalt (groundmass, nitric acid treatment), sample KAP-815 (#21814B-01)
0.61 ± 0.03 Ma
Integrated Age = 0.67 ± 0.03 Ma
Upper Kasurein Basalt (groundmass, nitric acid treatment), sample KAP-815 (#21814-02)
0.60 ± 0.05 Ma
Integrated Age = 1.50 ± 0.03 Ma
Cumulative %39Ar

the Baringo Trachyte. Because the best age obtained here for the Lake Baringo Trachyte flow was derived from complex multi-phase matrix material in contrast to phenocrystic anorthoclase in the case of the SCTF ages for the Pumice Tuff, we believe the latter are more reliable and should be used as the reference age for the Lake Baringo Trachyte.

Two samples of the Upper Kasurein Basalt were examined by the LIH method (Figures 7 and 8). Sample S15-3 demonstrated broad plateaux with and without dilute HF treatment in all three experiments. Plateau ages range from 0·560 to 0·514 Ma. An ''inverse'' isochron analysis of all plateau steps taken together suggests an age of 0·545 ± 0·014 Ma (n=38, MSWD=1·1, $(^{40}Ar/^{39}Ar)_{\text{``trapped''}}$=296·2 ± 0·9). The second sample yielded plateaux in four of five LIH experiments (KAP-815, with and without dilute HNO_3 acid wash). Plateau ages range from 0·540 to 0·610 Ma. An isochron analysis of all plateau steps yielded an apparent age of 0·565 ± 0·019 Ma (n=45, MSWD=0·8, $(^{40}Ar/^{39}Ar)_{\text{``trapped''}}$= 295·9 ± 0·6). Neither of these isochron ages are statistically distinguishable from each other, or from the age of the underlying Lake Baringo Trachyte. The ''best'' age of the Upper Kasurein Basalt is probably the weighted mean of the isochron ages for the two samples, giving 0·552 ± 0·015 Ma. HF and HNO_3 acid washes applied during the sample preparation stage generally resulted in increased radiogenic argon percentages of most gas mixtures relative to untreated samples, with consequent improvement in precision, but did not change the plateau ages noticeably. Previous K–Ar results on this lava flow reported by Cornelissen *et al.* (1990) indicated an apparent age of 0·8 Ma. This is demonstrably too old, given that the Upper Kasurein Basalt lies above the well-dated Lake Baringo Trachyte/Pumice Tuff at 0·543 ± 0·004 Ma, and that the basalt most likely occurs within the Brunhes Chron.

Anorthoclase phenocrysts from two samples of fluvially reworked Grey Tuff were dated herein by the SCTF ^{40}Ar/^{39}Ar technique; KAP-15 from JKS (GnJh-20) yielding an age of 0·51 ± 0·04 Ma, and KAP-23 from the Lion Site (GnJh-23) at 0·509 ± 0·009 Ma. These ages are indistinguishable, and combined yield a weighted mean age of 0·509 ± 0·009 Ma. The stratigraphic position of hominids KNM-BK 63-67 is about 0·7 m and KNM-BK 8518 is about 3 m below the Grey Tuff (Leakey *et al.*, 1969; Van Noten & Wood, 1985; Wood & Van Noten, 1986). Based on our dates for the Grey Tuff and underlying Pumice Tuff, we estimate the age of these hominids to be ~0·510–0·512 Ma, based on an inferred sedimentation rate of 1 m/ka for the 34 ± 13 ka duration of the interval between the two tuffs.

Considerable field and laboratory effort was spent attempting to locate high quality datable volcanic material from the Bedded Tuff (K4), without success. Plagioclase crystals extracted from a sand-sized tephra bed within the bedded tuff (S15-1) sampled 100 m north of site of GnJh-15 yielded the imprecise but geologically reasonable weighted-mean ages of 0·34 ± 0·24 Ma on single crystals, and 0·52 ± 0·19 Ma on fusion of five grains as a single population (Figure 6). The altered, glassy material comprising the bulk of the tephra proved undateable.

However, a pumiceous, air-fall trachytic tephra occurring high in the stratigraphy at collecting locality NRS on the northern bank of the Ndau River (see Figure 1) provided the opportunity to constrain the timing of deposition of the upper

Figure 8. Results of LIH analyses for the Upper Kasurein Basalt (K3^a) of the Kapthurin Formation.

Table 3 **Summary dating results, showing the previous best K-Ar age estimate, and the new $^{40}Ar/^{39}Ar$ results**

Unit	Name	Previous age (Ma ± 1 σ)	Revised age (Ma ± 1 σ)
—	Kampi ya Samaki Beds	0·23 ± 0·06*	0·235 ± 0·002
K4	Bedded Tuff	—	0·284 ± 0·012
GT	Grey Tuff	—	0·509 ± 0·009
K3[a]	Upper Kasurein Basalt	0·8†	0·552 ± 0·015
K2[a]	Lake Baringo Trachyte	0·58 ± 0·04†	0·545 ± 0·003
K2	Pumice Tuff	0·62 ± 0·06†	0·543 ± 0·004
J1[e]	Lower Kasurein Basalt	1·2†	0·61 ± 0·04

*Cornelissen *et al.* (1990).

†J. A. Miller cited in Tallon (1976). K-Ar ages cited for J. A. Miller have not been modified with respect to revised isotopic constants (Steiger & Jäger, 1977), since the original constants used were not reported. A correction factor of 1·0268 may be a close approximation (Dalrymple, 1979).

part of the Bedded Tuff member (K4) more precisely. Anorthoclase phenocrysts extracted from sub-2 cm pumice from this unit (MCB97-2p) yielded an age of 0·271 ± 0·013 Ma, while anorthoclase grains obtained from the bulk tephra yielded 0·291 ± 0·010 Ma (Figure 6). These two ages are statistically indistinguishable at the 95% confidence level, and give an overall weighted-mean age of 0·284 ± 0·012 Ma. This is the only known occurrence of siliceous pumice in the Kapthurin Formation between the Ndau and Kasurein rivers following deposition of the Grey Tuff. MCB97-2 may represent an early manifestation of the magma system that gave rise to the siliceous air-fall tephra of the upper Kampi-ya-Samaki Beds exposed at locality JLC 12 km to the northeast.

Anorthoclase from a sample of pumiceous air-fall tephra obtained from the Kampi-ya-Samaki Beds at sampling locality JLC at the northeastern edge of the village of Kampi ya Samaki (CYS97-1) provided the precise SCTF age of 0·235 ± 0·002 Ma (Figure 6). This confirms two earlier K–Ar ages on a sample of the upper Kampi-ya-Samaki Beds from approximately the same locality obtained by J. A. Miller (Tallon, 1976), with a weighted-mean age of 0·23 ± 0·06 Ma. This is the stratigraphically highest radiometric age obtained from the Kapthurin Formation or its equivalents in the Kampi-ya-Samaki Beds. The Bedded Tuff (K4) is overlain by yet another member of the Formation, the Upper Silts and Gravels (K5). The Kampi-ya-Samaki Beds, the lateral equivalent of the Bedded Tuff (K4) is overlain by the Loboi Silts, which contain Holocene archaeological and faunal remains (Farrand *et al.*, 1976). A summary of the dating results are provided in Table 3.

Implications for human evolution

Pumice Tuff (K2) to Grey Tuff interval

The new $^{40}Ar/^{39}Ar$ dates reported here for the Pumice and Grey tuffs definitively establish the age of fossil hominids KNM-BK 63-67 and KNM-BK 8518 at between 0·543 ± 0·004 and 0·509 ± 0·009 Ma. Given their stratigraphic position 0·7 and 3 m below the Pumice Tuff, a reasonable estimate of their age is 0·510–0·512 Ma. Few other Middle Pleistocene hominids are reliably dated. The Kapthurin hominids are younger than those from Bodo, Ethiopia, which have been dated by the $^{40}Ar/^{39}Ar$ method at between 640–550 ka (Clark *et al.*, 1994). OH 11, OH 23, and the Ndutu

cranium, from Olduvai Gorge, Tanzania have been estimated to date to 490–780 ka (White, 2000; Delson & van Couvering, 2000), and may thus be the near contemporaries of the Kapthurin hominids, but their precise ages remain uncertain. The best apparent age calibration of the upper Olduvai sequence is that of Tamrat *et al.* (1995), who maintain that the Norkilili Member of the Masek Beds has reversed paleomagnetic polarity, and so assign pre-Brunhes ages to the Masek beds. This conclusion is based on a single sample, however, and must be considered tentative.

Mandibular and dental remains preserve little information useful for diagnosis of species within the genus *Homo*, but mandibles KNM-BK-67 and KNM-BK-8518 have a generally archaic morphology and lack chins, excluding them from *H. sapiens*. KNM-BK-63, a right metatarsal, and KNM-BK-64, a proximal phalanx, likewise are archaic in appearance. Ulna KNM-BK-65, however, exhibits characters seen in *H. sapiens* as well as more archaic features (McBrearty *et al.*, 1999). These hominids have been referred to *H. erectus* by Wood (1991) and to "archaic" *H. sapiens* by Stringer (1993). McBrearty & Brooks (2000) have suggested the resumption of the use of *H. rhodesiensis* for Kabwe and related specimens such as the Bodo and Kapthurin material.

Pumice Tuff (K2) to Upper Kasurein Basalt interval

This part of the section is referred to the Middle Silts and Gravels lacustrine facies (K3′). Results described here demonstrate an 2σ age interval of 0·55–0·52 Ma. K3′ sediments are exposed in a small area adjacent to the Bartekero River, bounded on the east and north by outcrops of Upper Kasurein Basalt, and on the south by an isolated plug of Lower Kasurein Basalt (Figure 1). They include clays, sands, and fine conglomerates, often iron stained and exhibiting black mottling. They have been interpreted by Tallon (1976) to represent a lakeshore environment, and occasional rootcasts and small paleochannel features confirm the impression of fluctuating lake levels (McBrearty *et al.*, 1996). Fossil fauna includes aquatic forms as well as arid environmental indicators. The absence of crocodile, the presence of fish species tolerant of brackish conditions, and the occurrence of zeolites and fluorite suggest that the lake was saline and at times highly alkaline (McBrearty, 1999; Renaut *et al.*, 1999).

Ten archaeological sites, GnJh-41, GnJh-42, and GnJh-57 among them, are found in K3′ sediments. Surface collection to date has produced a small sample of artefacts (n=369). Most of these sites, with samples numbering only between 10 and 60 pieces, can perhaps best be considered "scatters between the patches" in the sense of Isaac *et al.* (1981). The K3′ artefact suite consists primarily of an informal flake industry made on small cobbles. Handaxes are rare, making up only 1·1% of the total sample. If abraded pieces, probably derived from higher in the section, are excluded, their frequency drops to 0·5%. The rarity of handaxes is notable in this time range, when the Acheulian industry is widespread in East Africa.

The Grey Tuff to Bedded Tuff (K4) interval

Sediments in this interval are referred to the Middle Silts and Gravels Member (K3) of the Kapthurin Formation. Tallon (1976) believed an unconformity to lie in this part of the section, though he failed to establish its precise field location. Results of our ^{40}Ar/^{39}Ar analysis show that this stratigraphic interval represents the time period from 0·509 ± 0·009 Ma, the age of the Grey Tuff, to 0·284 ± 0·012 Ma, the age of the trachytic Bedded Tuff unit sampled at locality NRS. The upper age limit for this interval was formerly thought to be ∼235 ka, based upon whole-rock K/Ar analysis of samples

from the Kampi-ya-Samaki Beds from near JLC reported by Tallon (1976). This date is frequently cited as the upper limit for the Acheulian industry in Africa. While our results confirm the estimate of ~235 ka for this unit, $^{40}Ar/^{39}Ar$ age determinations for material from within the Bedded Tuff (K4) section at NRS indicate a greater antiquity for underlying units than previously appreciated. The upper age limit reported here for the Acheulian in the Kapthurin Formation is therefore 284 ka, and this estimate also provides a minimum age for the Levallois technique, the well-executed blades, and the unusual "unifaces" at sites in the formation such as GnJh-03. The latter artefacts are broad ovate handaxes made on Levallois flake preforms. They have been transformed into handaxes with minimal retouch, and often the ventral face is untrimmed (Leakey *et al.*, 1969; Cornelissen, 1992; McBrearty *et al.*, 1996; McBrearty, 1999, 2001).

Geochemical analyses of K4 tephra reported by Tryon & McBrearty (2002) demonstrate that Middle Stone Age artefacts, including points and finely made Levallois debitage from sites such as GnJh-17, GnJh-63, and GnJi-28 (Rorop Lingop) underlie both dated units and are thus of a similar age. This previously unappreciated stratigraphic relationship combined with the new dates reported here shows that the Acheulian–Middle Stone Age transition occurred before 284 ka in this region of East Africa. Prior to this finding, the oldest date for the MSA in East Africa was a K–Ar estimate of 235 ± 5 from Gademotta, Ethiopia, reported by Wendorf *et al.* (1994). New dates for the Kapthurin Formation thus expand the age range of the East African MSA by 49 ± 13 ka.

The red ochre at site GnJh-15, which lies immediately below the Bedded Tuff (K4), is shown here to be of equal antiquity. Pigment at this site consists of an excavated sample from *in situ* context of more than 70 items with a total weight of >5 kg; these range in size from pulverized granular material weighting <3 g to large chunks >250 g (McBrearty & Brooks, 2000). The GnJh-15 pigment predates by a substantial margin the red ochre from Middle Stone Age sites in South Africa, dated by a variety of methods to ~120 ka at sites such as Klasies River (Singer & Wymer, 1982; Deacon, 1989) and to ~70 ka at Blombos (Henshilwood *et al.*, 2001) or the ochre from Twin Rivers, Zambia, dated by U-series on speleothem to ~230 ka (Barham & Smart, 1996; Barham, 1998). The African Middle Stone Age is notable for the earliest indication of symbolic behaviors (McBrearty & Brooks, 2000). The use of red ochre implies symbolic behavior and the early pigment from the Kapthurin Formation confirms an impression of human behavioral modernity early in the African record.

Acknowledgements

Work in Baringo was conducted under a research permit from the Government of the Republic of Kenya (Permit OP/13/001/C 1391/), and a permit to excavate from the Minister for Home Affairs and National Heritage, both issued to Andrew Hill and the Baringo Paleontological Research Project. Funding for field work was provided by grants to S.M. from the US National Science Foundation (SBR-9601419, SBR-9408926, DBS-9213775). We would like to thank Andrew Hill (Yale University), John Kingston (Emory University), and Christian Tryon (University of Connecticut) for their indispensable contributions to this work. Kingston supplied Figure 3 and Tryon provided Figure 1.

References

Barham, L. S. (1998). Possible early pigment use in south-central Africa. *Curr. Anthrop.* **39,** 703–710.

Barham, L. S. & Smart, P. (1996). Early date for the Middle Stone Age of central Zambia. *J. hum. Evol.* **30,** 287–290.

Best, M. G., Christiansen, E. H., Deino, A. L., Grommé, C. S. & Tingey, D. G. (1995). Emplacement of the large volume, rhyolitic Pahrangat ash-flow tuff, Nevada: 40Ar/39Ar chronology, paleomagnetism, and petrology. *Jour. Geophys. Res.* **100,** 24593–24609.

Bishop, W. W., Spooner, E. & Buckland, P. (1969). Kampi-ya-Samaki Beds. Unpublished report.

Bishop, W. W., Chapman, G. R., Hill, A. & Miller, J. A. (1971). Succession of Cainozoic vertebrate assemblages from the northern Kenya Rift Valley. *Nature* **233,** 389–394.

Chapman, G. R. & Brook, M. (1978). Chronostratigraphy of the Baringo Basin, Kenya. In (W. W. Bishop, Ed.) *Geological Background to Fossil Man*, pp. 207–224. Edinburgh: Scottish Academic Press.

Chapman, G. R., Lippard, S. J. & Martyn, J. E. (1978). The stratigraphy and structure of the Kamasia Range, Kenya Rift Valley. *J. Geol. Soc. Lond.* **135,** 265–281.

Clark, J. D., de Heinzelin, J., Schick, K. D., Hart, W. K., White, T. D., WoldeGabriel, G., Walter, R. C., Suwa, G., Asfaw, B., Vrba, E. & HaileSelassie, Y. (1994). African *Homo erectus*: old radiometric ages and young Oldowan assemblages in the Middle Awash valley, Ethiopia. *Science* **264,** 1907–1910.

Cornelissen, E., Boven, A., Dabi, A., Hus, J., Ju Yong, K., Keppens, E., Langohr, R., Moeyersons, J., Pasteels, P., Pieters, M., Uytterschaut, H., Van Noten, F. & Workineh, H. (1990). The Kapthurin Formation revisited. *Afr. Archaeol. Rev.* **8,** 23–76.

Cornelissen, E. (1992). Site GnJh-17 and its implications for the archaeology of the middle Kapthurin Formation, Baringo, Kenya. Musée Royale de l'Afrique Centrale, Annales, Sciences Humaines 133, Tervuren.

Dagley, P., Mussett, A. E. & Palmer, H. C. (1978). Preliminary observations on the palaeomagnetic stratigraphy of the area west of Lake Baringo, Kenya. In (W. W. Bishop, Ed.) *Geological Background to Fossil Man*, pp. 361–373. Edinburgh: Scottish Academic Press.

Dalrymple, G. B. (1979). Critical tables for conversion of K–Ar ages from old to new constants. *Geology* **7,** 558–560.

Deacon, H. J. (1989). Late Pleistocene paleoecology and archaeology in the southern Cape. In (P. Mellars & C. B. Stringer, Eds) *The Human Revolution: Behavioral and Biological Perspectives on the Origins of Modern Humans*, pp. 547–564. Edinburgh: Edinburgh University Press.

Deino, A. & Potts, R. (1990). Single crystal ^{40}Ar/^{39}Ar dating of the Olorgesailie Formation, southern Kenya Rift. *J. Geophys. Res.* **95,** 8453–8470.

Deino, A. L. & Hill, A. (2002). ^{40}Ar/^{39}Ar dating of Chemeron Formation strata encompassing the site of hominid KNM-BC 1, Tugen Hills, Kenya. *J. hum. Evol.* **1/2,** 141–151.

Deino, A. L., Tauxe, L., Monaghan, M. & Drake, R. (1990). 40Ar/39Ar age calibration of the litho- and paleomagnetic stratigraphies of the Ngorora Formation, Kenya. *J. Geol.* **98,** 567–587.

Delson, E. & Van Couvering, J. A. (2000). Composite stratigraphic chart of Olduvai Gorge. In (E. Delson, I. Tattersall, J. A. Couvering & A. S. Brooks, Eds) *Encyclopedia of Human Evolution and Prehistory*, p. 488. New York: Garland.

Farrand, W. R., Redding, R. W., Wolpoff, M. H. & Wright, H. T. (1976). *An Archaeological Investigation on the Loboi Plain, Baringo District, Kenya*. Technical Reports, 4. Ann Arbot, MI: University of Michigan Museum of Anthropology.

Fleck, R. J., Sutter, J. F. & Elliot, D. H. (1977). Interpretation of discordant 40Ar/39Ar age-spectra of Mesozoic tholeiites from Antarctica. *Geochimica Cosmica Acta* **41,** 1532.

Fuchs, V. E. (1950). Pleistocene events in the Baringo basin. *Geol. Mag.* **87,** 149–174.

Gregory, J. W. (1896). *The Rift Valley and Geology of East Africa*. London: Murray.

Henshilwood, C. S., Sealy, J. C., Yates, R., Cruz-Uribe, K., Goldberg, P., Grine, F. E., Klein, R. G., Poggenpoel, C., van Kiekerk, K. & Watts, I. (2001). Blombos Cave, southern Cape, South Africa: Preliminary report of the 1992–1993 excavations of the Middle Stone Age levels. *J. Archaeol. Sci.* **28,** 421–448.

Hill, A., Drake, R., Tauxe, L., Monaghan, M., Barry, J. C., Behrensmeyer, A. K., Curtis, G., Jacobs, B. F., Jacobs, L., Johnson, N. & Pilbeam, D. (1985). Neogene palaeontology and geochronology of the Baringo Basin, Kenya. *J. hum. Evol.* **14,** 759–773.

Hill, A., Curtis, G. & Drake, R. (1986). Sedimentary stratigraphy of the Tugen Hills, Baringo District, Kenya. In (L. E. Frostick, R. W. Renaut, I. Reid & J.-J. Tiercelin, Eds) *Sedimentation in the African Rifts*, pp. 285–295. Oxford: Blackwell. Geological Society of London Special Publication 25.

Isaac, G. Ll., Harris, J. W. K. & Marshall, F. (1981). Small is informative: the application of the study of mini-sites and least-effort criteria in the interpretation of the early Pleistocene archaeological record at Koobi Fora, Kenya. In (J. D. Clark & G. Ll. Isaac, Eds) *Las Industrias Mas Antiguas: X Congresso Union International De Ciencias Prehistoricas y Protohistoricas*, pp. 101–119. Mexico City.

Leakey, L. S. B. (1955). The climatic sequence of the Pleistocene in Africa. In (L. Balout, Ed.) *Actes De La IIe Session Du Congrès Panafricain De Préhistorire, Alger, 1952*, pp. 293–294. Paris.

Leakey, M., Tobias, P. V., Martyn, J. E. & Leakey, R. E. F. (1969). An Acheulian industry with prepared core technique and the discovery of a contemporary hominid at Lake Baringo, Kenya. *Proc. Prehist. Soc.* **35,** 48–76.

Martyn, J. (1969). The geologic history of the country between Lake Baringo and the Kerio River, Baringo District Kenya. Ph.D. Dissertation, University of London.

McBrearty, S. (1999). Archaeology of the Kapthurin Formation. In (P. Andrews & P. Banham, Eds) *Late Cenozoic Environments and Hominid Evolution:*

a Tribute to Bill Bishop, pp. 143–156. London: Geological Society.

McBrearty, S. (2001). The Middle Pleistocene of East Africa. In (L. H. Barham & K. Robson-Brown, Eds) *Human Roots: Africa and Asia in the Middle Pleistocene*, pp. 81–97. Bristol, UK: Western Academic & Specialist Press.

McBrearty, S. & Brooks, A. S. (2000). The revolution that wasn't: a new interpretation of the origin of modern human behavior. *J. hum. Evol.* **39,** 453–563.

McBrearty, S., Bishop, L. & Kingston, J. (1996). Variability in traces of middle Pleistocene hominid behavior in the Kapthurin Formation, Baringo, Kenya. *J. hum. Evol.* **30,** 563–580.

McBrearty, S., Brown, B., Deino, A., Kingston, J. D. & Ward, S. (1999). Anatomy, context, age, and affinities of hominids from the Kapthurin Formation, Baringo, Kenya. *J. hum. Evol.* **36,** A12.

McCall, G. J. H., Baker, B. H. & Walsh, J. (1967). Late Tertiary and Quaternary sediments of the Kenya Rift Valley. In (W. W. Bishop & J. D. Clark, Eds) *Background to Evolution in Africa*, pp. 191–220. Chicago: University of Chicago Press.

Renaut, R. W., Ego, J., Tiercelin, J.-J., Le Turdu, C. & Owen, R. B. (1999). Saline, alkaline palaeolakes of the Tugen Hills-Kerio Valley region, Kenya Rift Valley. In (P. Andrews & P. Banham, Eds) *Late Cenozoic Environments and Hominid Evolution: a Tribute to Bill Bishop*, pp. 41–58. London: Geological Society of London.

Renne, P. R., Sharp, W. D., Deino, A. L., Orsi, G. & Civetta, L. (1998). $^{40}Ar/^{39}Ar$ dating into the historic realm. *Science* **277,** 1279–1280.

Samson, S. D. & Alexander, E. C. Jr (1987). Calibration of the interlaboratory $^{40}Ar/^{39}Ar$ dating standard, MMhb-1. *Chem. Geol. Isot. Geosci.* **66,** 27–34.

Sharp, W. & Deino, A. L. (1996). CO_2 laser heating of samples for Ar–Ar geochronology. *EOS* **77,** F773.

Singer, B. S. & Pringle, M. S. (1996). The age and duration of the Matuyama-Brunhes geomagnetic polarity reversal from $^{40}Ar/^{39}Ar$ incremental heating analyses of lavas. *Earth Planet. Sci. Lett.* **139,** 47–61.

Singer, R. & Wymer, J. (1982). *The Middle Stone Age at Klasies River Mouth in South Africa*. Chicago: University of Chicago Press.

Steiger, R. H. & Jäger, E. (1977). Subcomission on geochronology: Convention on the use of decay constants in geo- and cosmochronology. *Earth Planet. Sci. Lett.* **36,** 359–362.

Stringer, C. B. (1993). New views on modern human origins. In (T. D. Rasmussen, Ed.) *The Origin and Evolution of Humans and Humanness*, pp. 75–94. Boston: Jones & Bartlett.

Tallon, P. (1976). The Stratigraphy, palaeoenvironments and geomorphology of the Pleistocene Kapthurin Formation, Kenya. Ph.D. dissertation, University of London.

Tallon, P. (1978). Geological setting of the hominid fossils and Acheulian artifacts from the Kapthurin Formation, Baringo District, Kenya. In (W. W. Bishop, Ed.) *Geological Background to Fossil Man*, pp. 361–373. Edinburgh: Scottish Academic Press.

Tamrat, E., Thouveny, N., Taieb, M. & Opdyke, N. D. (1995). Revised magnetostratigraphy of the Plio-Pleistocene sedimentary sequence of the Olduvai Formation (Tanzania). *Palaeogeogr., Palaeoclimatol., Palaeoecol.* **114,** 273–283.

Tauxe, L., Monaghan, M., Drake, R., Curtis, G. & Staudigel, H. (1985). Paleomagnetism of Miocene East African Rift sediments and the calibration of the Geomagnetic Reversal Time Scale. *J. geophys. Res.* **90,** 4639–4646.

Taylor, J. R. (1982). *An Introduction to Error Analysis.* Mill Valley, CA: University Science Books.

Thomson, J. (1884). *Through Masailand*. London: Samson Low.

Tryon, A. C. & McBrearty, S. (2001). Tephrostratigraphy and the Acheulian to Middle Stone Age transition of the Kapthurin Formation, Baringo, Kenya. *J. hum. Evol.* **1/2,** 211–235.

Van Noten, F. (1982). New Acheulian sites and a new hominid from Kapthurin. *Nyame Akuma* **21,** 11–12.

Van Noten, F. & Wood, B. (1985). Un nouvel hominide à Baringo, Kenya. *L'Anthropologie* **89,** 141–143.

Van Noten, F., Cornelissen, E., Gysels, J., Moeyersons, J., Nijs, K. & Uytterschaut, H. (1987*a*). The Kapthurin Project, Baringo: the 1984 season. *Nyame Akuma* **28,** 20–27.

Van Noten, F., Cornelissen, E., Gysels, J., Moeyersons, J. & Uytterschaut, H. (1987*b*). The Kapthurin Project, Baringo: the 1985 season. *Nyame Akuma* **29,** 36–41.

Van Noten, F., Moeyersons, J. & Gysels, J. (1983). Kapthurin, een archaeologisch project aan het Baringo-meer, Kenya. *Africa Tervuren* **29,** 1–15.

Walsh, J. (1969). *Geology of the Eldama Ravine, Kabarnet Area*. Report, 84. Nairobi: Geological Survey of Kenya.

Wendorf, F., Close, A. E. & Schild, R. (1994). Africa in the period of *Homo sapiens neanderthalensis* and contemporaries. In (S. J. De Laet, A. H. Dani, J. L. Lorenzo & R. B. Nunoo, Eds) *History of Humanity, Vol. 1: Prehistory and the Beginnings of Civilization*, pp. 117–135. New York: Routledge & UNESCO.

White, T. D. (2000). Olduvai Gorge. In (E. Delson, I. Tattersall, J. A. Van Couvering & A. S. Brooks, Eds) *Encyclopedia of Human Evolution and Prehistory*, pp. 486–489. New York: Garland/Taylor & Francis.

Wood, B. (1991). *Koobi Fora Research Project, Volume 4: Human Cranial Remains*. Oxford: Oxford University Press.

Wood, B. A. & Van Noten, F. L. (1986). Preliminary observations on the BK 8518 mandible from Baringo, Kenya. *Am. J. phys. Anthrop.* **69,** 117–127.

Yamei, H., Potts, R., Baoyin, Y., Zhengtang, G., Deino, A., Wei, W., Clark, J., Guangmao, X. & Weiwen, H. (2000). Mid-Pleistocene Acheulean-like stone technology of the Bose Basin, South China. *Nature* **287,** 1622–1626.